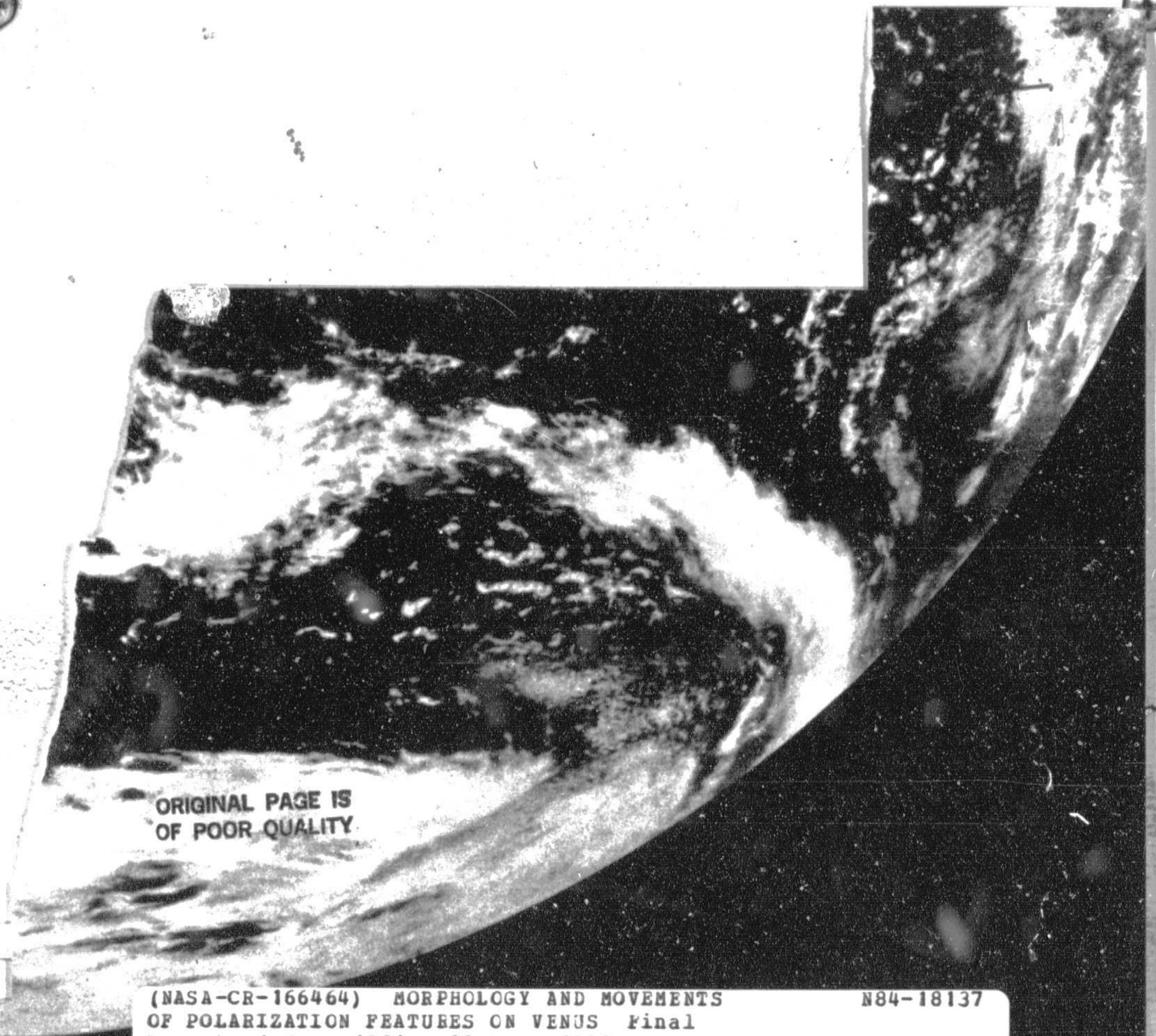

(NASA-CR-166464) MORPHOLOGY AND MOVEMENTS OF POLARIZATION FEATURES ON VENUS Final Report, 1 Jan. 1981 - 30 Nov. 1982 (Wisconsin Univ.) 86 p HC A05/MF A01 CSCL 03B G3/91

N84-18137

Unclas 00676

A REPORT

from the space science and engineering center
the university of wisconsin-madison
madison, wisconsin

Morphology and Movements of Polarization Features on Venus

NASA Grant # NAG 2-93

Morphology and Movements of Polarization Features on Venus

NASA Grant # NAG 2-93

Final Report

1 January 1981 to November 30, 1982

Sanjay S. Limaye

Principal Investigator

Space Science & Engineering Center
University of Wisconsin-Madison
1225 West Dayton Street
Madison, Wisconsin 53706
(608) 262-9541

Table of Contents

Abstract

Ground and spacecraft based polarization observations of Venus had detected the signature of the so called 1-micron radius cloud particles that constitute the main cloud deck on Venus, as well that of sub-micron sized particles that form a haze above this main cloud layer. Whether such observations showed any local clustering or organization in the polarimetry data remained uncertain until the relatively high resolution observations from the Pioneer Venus Orbiter Cloud Photopolarimeter (OCPP) became available. This investigation concerned itself towards studying the available polarization data from this instrument to see whether local organization was present, to study the morphology of such features or polarization clouds, and finally, to see if they can be followed in a sequence of observations to study their motions.

The results are as follows: (i) the polarization observations do show local, organized features whose morphology is similar to that of the ultraviolet clouds, (ii) their lifetimes (for features of several thousand km size) is at least on the order of a day, (iii) the large scale features show the same retrograde motions as do the ultraviolet clouds. The speed of such movements is approximately 100 ms-1, quite comparable to that of the ultraviolet clouds. (iv) the direction of polarization (i.e. the angle which the electric field vector makes with the local scattering plane) also shows "features" which are correlated with the polarization features as well as the ultraviolet clouds, at

some phase angles. (v) the contrast, defined in terms of the departure from a simple scattering law such as Minnaert's scattering law, shows that it is maximum around 60° phase angle and then gradually decreases with higher and lower phase angles. The contrast reaches a value of about 30 % at the shortest wavelength at maximum.

1. Introduction

Polarization studies of Venus have been crucial in learning the nature of the clouds on Venus. The ability to obtain a decent phase angle coverage from earth based telescopes albeit at relatively low spatial resolution has been a deciding factor in these studies (Lyot (1929), Hansen and Hovenier (1974), Kawabata and Hansen (1977), Travis (1977), Dollfus et al. (1979), Lane (1979), Esposito and Travis, 1982. Almost all of these studies however were restricted to finding the microphysical properties of the clouds and haze layers on Venus. The relatively high spatial resolution for polarimetry data offered by the Pioneer Venus Cloud Photopolarimeter (OCPP) has been beneficial in this regard as well.

The low spatial resolution of the earth based polarimetric observations precluded regional or local scale studies of the features seen in these observations although the observations of Lyot indeed suggested that such organization was probable. It was long suspected that these features were formed by some type of clouds. What was not known was how stable was the morphology of these features, how were they formed? What was the relationship with the dark ultraviolet clouds seen in the unpolarized light? These and other questions could be answered only after the greater spatial and temporal resolution observations from the Pioneer Venus mission became available.

The Pioneer Venus missions have been described by Colin and Hunten (1977) and by Colin (1979). The Orbiter Cloud Photopolarimeter instrument has been described by Russel et al. (1977) and by Travis (1979). Results on the polarimetry as well as the imaging investigations performed from the data obtained by this instrument have been presented by Travis et al. (1979a,b), Rossow et al. (1980), Kawabata et al. (1980) and also by Esposito and Travis (1982), Limaye et al. (1982) and Del Genio and Rossow (1982). Early results from the present investigation were presented by Limaye (1982a,b).

This report describes in detail the results obtained on the regional structure of the detail seen in the polarization data in terms of both magnitude and direction, their life times and the ability to follow them over a period of time, as well as their relationship with the ultraviolet clouds.

2. The Polarimetry Data

a. The OCPP Instrument

The polarimetry data on Venus used in this work was obtained by the Pioneer Venus OCPP instrument during the nominal and extended missions (8 December 1978 to 27 July 1980). Data was obtained on nearly 180 orbits during this period and was analyzed. The data coverage is not continuous in time due to several reasons- the chief ones being the fact that OCPP is also used to perform imaging investigation, and secondly the phase angle coverage varies as Venus moves around in its orbit and thus no data is obtained when the OCPP is able to view only its night side. Finally, ground reception of the data transmitted from the Pioneer Venus Orbiter is not always possible due to conflicts with other space missions. The detailed working of the OCPP instrument is described by Russel et al. (1977) and by Travis (1979). However, for the sake of completeness a brief summary is presented below.

The Pioneer Venus Orbiter spacecraft moves around Venus in a highly elliptic orbit (eccentricity=0.845) inclined at about 105° with the orbital plane. The periapsis point is located in the Venus northern hemisphere at approximately 20° latitude. The OCPP instrument primarily consists of a Dall-Kirkham telescope with a 3.7 cm aperture and a 17.5 cm focal length. The telescope is mounted near the periphery of the drum shaped orbiter spacecraft that is spin stabilized at a nominal rate of 5 RPM. The principal axis of the telescope is in the plane containing the spacecraft spin axis, and can be pointed at many discrete positions between 45 and 135° angle with the positive spin axis of the spacecraft. The spacecraft attitude is maintained so that the positive spin axis of the spacecraft points towards the south ecliptic pole. Thus, as the Orbiter moves around Venus in its orbit, the OCPP telescope field-of-view (FOV) is swept across the disk of Venus. The spacecraft motion results in the translation of such successive scans providing the necessary cross-scan coverage for full disk imaging. Due to the high ellipticity orbit the instantaneous range to Venus disk changes substantially which results in a substantial overlap of the successive scans near the apoapsis portion of the orbit, and a substantial underlap near the periapsis portion of the orbit. It is generally not necessary to step the telescope during the coverage of a single full disk observation.

The light gathered by the telescope passes through one of the 16 filters/retarders mounted on a rotatable wheel near the focal plane of the telescope. There are three filters each for four wavelengths: 270, 365, 550 and 935 nm. Another set of filters and retarders mounted in front of the filter wheel makes it possible to obtain polarimetry mode observations at the four wavelengths so that the retarder fast axis makes angles of 0, 22.5 and 45° relative to the instrument plane. A Wollaston birefringent prism divides the resultant light into two parts which are polarized at right angles to each other. A set of silicon photodiodes generate an electrical signal corresponding to each of the four wavelengths which is then digitized and then transmitted to earth. It takes three successive scans at each wavelength to determine the linear polarization and the direction of polarization along with the intensity. A fourth scan provides calibration data. Thus a total of 16 spacecraft rolls are required to acquire polarization data over the essentially same portion of Venus at four wavelengths. The relatively low resolution in the polarimetry mode (compared to the imaging mode) results in a very small change in the viewed scene over the 16 rolls of the Orbiter (6.5 x 8 mrad). A sample rate of 9.52 msec provides a maximum of 136 separate measurements in a single scan across Venus.

b. The OCPP Observations

Table I lists the full disk polarimetry maps used in this study. The observation time, the phase angle, the sub-spacecraft point on Venus, etc. are tabulated corresponding to the map center time (i.e. when the OCPP optic axis passes through the center of Venus during a full disk observation). The total phase angle coverage is quite good although the temporal coverage is rather sporadic. In many instances however more than two observations per 24 hour orbit were acquired thus enabling examination of the polarization features for a longer time. As was mentioned earlier, the possibility of following the polarization features over a period of time as indicators of atmospheric motion was one of the goals of this investigation, and for this purpose such coverage is important.

Figure 1 shows the phase angle coverage obtained in terms of full disk observations. It should be pointed out here that the phase angle at any point on the visible disk of Venus (to the Pioneer Orbiter spacecraft) can be somewhat different from its value for the Venus center due to the fact that the spacecraft is never more than approximately 11 Venus radii away from the planet, and is frequently closer for most of the OCPP observations. Consequently the phase angle in a given full disk observation can vary by as much as 6 to 18° over the disk of Venus about the phase angle at the center of Venus. For each map the amount of linear polarization (%), the unpolarized intensity, the celestial co-ordinates on Venus of each observation point, the cosines of zenith angles of the OCPP and the sun and the direction of polarization are available. The direction of polarization is the angle between the local scattering plane and the direction of vibration of the electric field vector. The local scattering plane is defined by the sun-OCPP and the point on Venus being observed. By convention, polarization is termed as positive if the direction of polarization is within 45° of the normal to the scattering plane, and negative if the direction is within 45° of the local scattering plane.

c. Data Format

For the purpose of studying the morphology of the poalrization features the polarization data (both the magnitude and direction) were represented as two dimensional images. The image representation of the data has several advantages: the images provide a convenient way looking at a large amount of data points on the planet at once, either on a image processing system where it can be easily manipulated, or as as hard copy. Additionally, time series of such images can be constructed to study the temporal evolution of the features and study their morphology and movements. The image representations of different quantities can be compared to see if there are any obvious relationships that can be further quantitatively studied, etc. In generating such image representations, where a given data number representing a given brightness is related to the observed quantity in some manner, it is necessary to use some known co-ordinates. In the present case the Venus (celestial) coordinates were used to construct two dimensional latitude longitude maps.

The nominal resolution for these maps was chosen to be 1o of latitude and longitude so that a full disk observation could be represented as an image with a size of 181 x 181 image elements, or a latitudinal coverage of 90°North to 90° South and a longitudinal coverage of 90° about the sub-solar point to the east and west. The relatively large field of view of the OCPP instrument however yields a data resolution of 2 to 5 times the map resolution over many parts of Venus. Thus many points in the map representation are unfilled due to lack of data. For cosmetic reasons therefore, these points are filled in by bi-linear interpolation of the observations about those points.

The simple rectangular map representation of the data produces severe distortations in the feature shapes at high latitudes and therefore the data were also mapped into polar stereographic projections for both the northern and the southern hemispheres as well. These polar projections make it easier to study the patterns of the cloud forms at higher latitudes.

Two types of scalings were used for the polarization amount to generate the image representations. First type of representation was the linear scaling of the polarization amount: the observed positive polarization amount was scaled into digital image brightness numbers between 129 and 255 and the negative polarization was scaled linearly between 0 and 127, with the 128 data number depicting the zero percent polarization amount. The maximum and minimum polarization amounts that determined the actual scale factors were determined for each observation and each wavelength separately in order to maximize the apparent contrast in the image rendition. The drawback of this type of scaling is that it is difficult to compare two different maps as they will in general have different scale factors.

In order to alleviate this problem, a second type of scaling was simultaneously used: logarithmic scaling. With this type of scaling the positive and negative polarization amounts were separately scaled logarithmically into two separate image renditions so that the data number range 0 to 255 spanned the polarization range 0.15 to 100 % logarithmically.

The direction of polarization as linearly scaled between data numbers 100 and 190 as follows:

$$\text{Data Number (DN)} = 100 + |\text{Direction}| \text{ (Degrees)}$$

The direction which can be between -90 and +90o is reduced to an absolute scale from 0 to 90o prior to scaling.

In order to facilitate comparison between the features seen in the polarization amounts, the direction of polarization and the unpolarized intensities (at least the two shortest wavelengths), the unpolarized intensities were also linearly scaled and rendered as images. Similar to the linear scaling of the polarization magnitude data, the observed intensities were scaled between 0 and 255, so that the scale factors were once again different for each map and each wavelength.

Finally, the image renditions of the polarization amount, the direction, and the unpolarized intensity in both the rectangular and polar representations were produced as a single composite product for each wavelength of each full disk observation. Figure 2 shows an example of such a composite for each wavelength of a single observation in each of the four wavelengths. The first row in each composite for a given wavelength represents the linearly scaled linear polarization amount. The left most sub-image represents a rectangular map from the north pole to the south pole and centered around the sub-spacecraft point. The two right column positions in this row represent respectively the northern and the southern hemispheres in polar projections centered about the respective poles. The latitude lines are thus concentric circles about the center point, with the equatorial circle touching the edges of the sub-image. The middle row represents the unpolarized intensity, with the rectangular map on the left and the two polar projections on the right in the same format as the polarization amount. The bottom row in each composite represents three rectangular projection maps-- the left one represents a logarithmically scaled rendition of the positive polarization, the middle one the negative polarization amounts, while the right most sub-image representing the variation of the direction of polarization over the disk, once again in the rectangular projection.

3. Results

The primary goal was to see if the polarization features were localized into discrete features, and whether they could be tracked. It is obvious from the data shown in Figure 2 that indeed detail can be seen in the polarization amount. Variation is seen on a local scale in the positive as well as negative polarization amounts. Whether the observed polarization is positive or negative depends not only on the wavelength of observation, but also on the nature of the scatterers in the atmosphere. The sub-micron sized haze reported by Travis et al. (1979) in the polar regions, for example, produces a positive polarization at 935 nm, as can be seen in Figure 2. It is also apparent that the structure seen in the polarization magnitude variation over the disk is somewhat similar to that seen in the unpolarized intensity data at least at the two short wavelengths. Examination of other OCPP observations taken at other phase angles also show similar features, but to a varying degree. Several examples are shown later in Figure 10. However, a great variability is seen in the "visibility" of such features at all wavelengths. At low and high phase angles the short wavelengths do not show detail to the same degree as at moderate phase angles (40-70°).

It could be expected that the sub-micron responsible for at least some of the detail seen in the 935 and 550 nm polarization data, was likely to be variable in terms of its thickness etc., but that in itself probably does not account for the enormous variability seen in the polarization features. It is quite likely that at least some of the features seen in the polarization data are related to the ultraviolet contrasts as has been suggested from time to time (see Travis, 1975). It is therefore necessary to understand what relationship if any exists between the ultraviolet contrasts and the polarization data.

3.1 OCPP intensity Data: Observed Contrasts

No detail in the appearance of Venus is seen at all but the shortest (ultraviolet) wavelengths. The OCPP data is available at two short (270 and 365 nm) and two long wavelengths (550 and 935 nm). Mariner 10 images of Venus taken through the orange filter did show some contrast near the edge of the bright polar cloud (in ultraviolet). The polarization data however shows a wealth of detail in not only the 550 nm channel but also the 935 nm data at moderate phase angles (50 to 70o). From the example shown in Figure 2 it is evident that at least some phase angles there is a substantial correlation between the features seen in the polarization amount and the short wavelength intensity data.

However, before the relationship between the the observed polarization features and those seen in the unpolarized intensity data can be quantitatively studied, the effects of the varying observing geometry on the data have to be removed. Kawabata (1981) has investigated the effects of such geometry variation on the polarization amounts. Unlike the ground bases observations, where the distance of the observer is very large compared to the radius of the planet, the Pioneer observations of Venus are obtained from a close proximity to Venus (32,000 to 66,000 Km approximately). Kawabata's results obtained by modelling the Venus atmosphere show that the observed polarization amount is sensitive to the ratio of the observer distance to the radius of the planet, and that the larger the ratio the smaller is the variation in observed polarization with the variation in the observer distance. These effects primarily arise out of differing scattering angles for differnt points on the planet's visible disk. Unfortunately, the dependence of the observed polarization on the scattering geometry cannot be easily modelled, and hence is not explicitly addressed in this study.

The situation with the unpolarized intensity data is fortunately somewhat simpler, where indeed the effects of the varying scattering geometry can be modelled with some ease to a large extent. This removal of the effects of scattering geometry or "normalization" is discussed next.

Intensity Normalization

The observed intensity at any point on Venus however varies substantially not only due to real albedo differences on Venus, but also in large part due to changing viewing geometry: the solar and OCPP zenith angles and the azimuth angles are different for each point on Venus. This spurious effect can be eliminated by "normalizing" the observed intensities to a standard geometry to reveal only the real albedo differences. Such normalization procedure has been previously used by Limaye and Suomi (1977) to elucidate cloud cover differences on Venus. This normalization procedure requires the use of a particular scattering model or law. In this case considering the large amount of phase angle coverage available at all four wavelengths, it was decided to consider the Minnaert Scattering law which depends only on the cosines of the illumination and viewing angles:

$$I\mu = a_o(\mu\mu_o)^k$$

or,

$$\ln(I\mu) = (\mu\mu_o) + \ln(a_o)$$

Thus, on a log-log plot, if the Minnaert law is applicable to the present case, $I\mu$ vs. $\mu\mu_o$ should produce a linear plot. A value of 1 for k corresponds to the case of Lambert's reflection law. Figure 3 shows several examples of such a plots for all the four wavelengths, and different phase angles. The solid lines in each case depict the least squares fit to the data. As is apparent from this figure, Minnaert law appears to be quite applicable to the data. The simplicity of the Minnaert scattering function and the apparent good quality fit to the data suggested that this law could be used adequately for removing the scattering geometry effects from the unpolarized intensities at all four wavelengths.

Usually one would expect that the normal albedo, or the Minnaert intercept would be constant over observations covering all phase angles. This however is not the case in the present situation. Figure 4 shows the variation of a_o for 270, 365, 550 and 935 nm as a function of phase angle. Note that the scale for the normal albedo is logarithmic. Up to 100° phase angle the variation in a_o is small. At 365 nm one can even detect the somewhat higher value of the normal albedo between 15 and 20° phase angle that is undoubtedly related to the cloud bow effect of the 1.1μ cloud particles. Beyond about 100° phase angle the normal albedo increases dramatically.

Most of this variation is however likely to be spurious due to several limiting factors. First of all, the high phase angle observations represent a predominant sampling of the high (southern) latitude regions of Venus in the OCPP data, and are thus somewhat biased. It is known that at short wavelengths the albedo of the cloud cover on Venus is higher by almost 50 % in the high latitude regions, and thus somewhat different Minnaert coefficients can be expected. Secondly, Minnaert law does not take into account the effect of the varying azimuth angle, and is thus unrealistic to some extent. Further, at these high phase angles Minnaert law is frequently inadequate to fully describe the limb darkening as is evident from the plots of I/μ versus $\mu\mu_o$ on a logarithmic scale, and from the coefficient of determination of the linear relationship between logarithm of $I\mu$ and $\mu\mu_0$. The variation of this coefficient (the linear correlation coefficient is given by the square root of this quantity) for the data analyzed is shown as a function of phase angle for the four wavelengths in Figure 5. As can be seen, the correlation between $\ln(I\mu)$ and $\ln(\mu\mu_0)$ decreases very rapidly beyond about 140° phase angle, but is quite good up to about 100° phase angle.

The dependence of k, the limb darkening exponent, is also found to have a small phase angle dependence for small to moderate values of phase angles as can be seen from Figure 6. The variation of k at the high phase angles can also be traced to the same problems as for the normal albedo, as discussed previously.

Contrast in Intensity Data

The use of a scattering law affords a side-benefit as well. The departure from the predicted intensity of the observed value for all points on the disk of Venus is a good measure of the "contrast". The use of such a definition allows one to easily calculate the contrast as a function of wavelength that is more objective a measure than by selecting the darkest and brightest points observed as is done usually. The second benefit is that at least in terms of the Minanert scattering law, where the coefficient a_o (representing the intercept on a log-log scale) is the intensity predicted for normal incidence and normal viewing (both μ and μ_0 = 1), its variation with phase angle is akin to the variation of normal "apparent" albedo with phase angle, or similar to the phase curve of Venus.

The fact that the contrast observed at the four OCPP wavelengths is phase angle dependent is indicated by the "spread" around the least squares fit line on the Minnaert plots (Figure 3). Note the greatly reduced scatter around the least squares fit line at the low phase angle observations (Figure 3a,b). In contrast to that at moderate phase angles a much greater scatter is seen about the least squares fit line at all wavelengths (Figure 3d,e,f). The contrast can thus be defined in one of two ways, relative to the average scattering function: an absolute departure from the intensity expected from the scattering law, or, a root mean square (RMS) deviation from the scattering law. Both the absolute contrast and the RMS contrasts are shown in Figure 7 (a and b respectively) as a function of disk center phase angle for the four wavelengths.

Pollack et al. (1980) and Esposito (1980) have also presented contrast measurements as a function of phase angle at 365 and 240 nm respectively. However, they calculate the contrast between the brightest and the darkest point on the planet as opposed to the departure from a scattering law. Even then, the functional dependence they obtain for the ensemble average of the maximum contrast determined from a number of OCPP images is similar to that presented here. Thus, the contrast peaks at 365 nm at around 60° phase angle and decreases almost linearly beyond that point as the phase angle increases. The polarimetry mode data indicate that the contrast can vary substantially at low phase angles and the variation is maximum at the two shorter wavelengths. At 270 nm the contrast peaks at around 50 to 60° phase angle, whereas at the two longer wavelengths, 550 and 935 nm the maximum contrast (approximately 4 %) is observed at approximately 140° phase angle. An interesting feature at these two longer wavelengths is the slightly enhanced contrast (around 2.5 %) in the unpolarized intensity at the cloud-bow phase angle of 18° for the 1.1 μ radius cloud particles.

The scatter seen in the contrast vs. phase angle plots is due both to the variable amount of contrast present on Venus as well as a temporal dependence as the clouds evolve. Further, no distinction has been made between the different solar azimuth angles for the observations. Thus any variation in the contrast at a given phase angle due to morning or evening hemisphere scattering geometry is also included in the figure. The RMS contrast shows the same behaviour as the absolute contrast at the four wavelengths.

3.2 Correlation between Observed Polarization and Contrast

The relationship between the observed polarization amount and the contrast (at least at the short wavelengths in the ultraviolet region where there is some observable contrast) has been of some interest for some time as it may provide a clue to the identity of the ultraviolet absorber(s) responsible for the observed contrasts. Until the Pioneer Venus OCPP data became available much confusion has existed regarding the possible relationship between the observed contrast and the associated polarization amount (Travis, 1975). The question often asked is whether the bright clouds have greater associated polarization than the dark clouds or vice versa? Esposito (1980) investigated this question from a limited amount of OCPP polarimetry data and found a marginally significant positive correlation between contrast and polarization at 270 and 365 nm ($r^2 = 0.10$ at 270 nm and $= 0.11$ at 365 nm). Thus, dark clouds have greater polarization and possibly point to a polarizing absorber. However, this correlation can also be explained (see Esposito and Travis, 1982) without requiring any polarizing absorber at all- the dark clouds are darker due to fewer photons, thus indicating less multiple scattering than bright clouds, and hence have a greater polarization which is largely due to singly scattered light.

The relationship between the observed polarization and the observed contrast in the unpolarized intensity data was investigated in the present study by determining the linear correlation coefficient between the observed polarization and the departure from the Minnaert scattering law for the unpolarized intensity for the observed point. Thus a positive value for the deviation corresponds to a "bright" feature and vice versa. The variation of the correlation coefficient between the magnitude of the observed polarization and the intensity deviation from the Minnaert law for each of the four wavelengths is shown in Figure 8a. Although the correlation is weak in all cases, a dependence on phase angle is apparent. The correlation between polarization and contrast is especially complex as it flip-flops between positive and negative values with phase angle. It is easy to see why the early results were often contradictory as they did not refer to specific phase angles. Nevertheless, the relationship between the observed contrast and the polarization remains a puzzle.

Esposito and Travis (1982) show that the observed polarization for the dark and bright (in the ultraviolet) clouds have different phase angle dependence at the shorter wavelengths. At 550 nm they report no difference between the dark and bright feature polarization. Their contrast data are obtained from the same meridian and is calculated from the darkest and brightest points on that meridian.

From an analysis of more data from both the Orbiter Ultraviolet Spectrometer (OUVS) and the polarimetry data from the OCPP instrument, Esposito and Travis have recently shown that the submicron haze and polarization are anticorrelated. The darker areas have slightly lower cloud tops (approximately 1.2 +/- 0.6 km) and the brighter areas have an excess haze over them. The results obtained in this study are consistent with this interpretation in many cases, although some exceptions have been noted. Presumably these apparent inconsistencies may be due not only in the amount of the haze material present but also due to variations in size distributions of the haze particles.

3.3 Correlation between Observed Polarization Amount and Direction of Polarization

Figure 8b shows the phase angle dependence of the correlation coefficient between the observed polarization amount (%) and the direction of polarization ($0 < \theta < 90°$). According to the convention, polarization is positive if the direction of polarization is within 45° of the normal to the scattering plane and negative if it is within 45° of the local scattering plane. As will become apparent, the polarization direction is observed to show localized features that correspond to the ultraviolet contrast features as well as the polarization magnitude features. It is therefore of interest to see what correlation exists between the direction of polarization and the polarization magnitude, as a function of phase angle. The curves in Figure 8 indicate that the correlation is phase dependent with a different behaviour at each wavelength. Except at 935 nm the correlation coefficient approaches perfect correlation ($r^2 = 1.0$) at many phase angles near 18° and 60° for 270 nm data, 18°, and 60-70° for the 365 nm data, and 18° and 150-160° for the 550 nm data. At 935 nm the maximum correlation observed is only 0.8 near 30° and 140° phase angle. At 365 nm the correlation decreases to 0.1 near 30, 110 and 150° phase angles. Similar decrease is observed for the 270 nm data as well although to a much less pronounced extent.

For the sake of completeness Figures 9(a,b,c) show the average direction of polarization, the absolute polarization amount and the average intensity as a function of phase angle, respectively. Note that the averages represent disk integrated values and are not area weighted.

3.4 Morphology of Polarization Features

Figure 10 presents a montage of 30 full disk observations roughly spaced at 5o phase angle for all four wavelengths. Along with the linear polarization, the unpolarized intensity maps at 270 and 365 nm are also presented (10e and 10f). The observation numbers are given in Table II. Note that all the polarization images were linearly scaled to represent both the positive and negative polarization amounts individually so that the same brightness does not necessarily represent the same polarization amount from map to map.

At 270 nm little detail is seen in most of the observations. There are several reasons for the low contrast seen at this wavelength in the polarization data. First of all, the sensitivity of the detector used at this wavelength is poor compared to say at 365 nm. This leads to a reduced ability to detect small changes in polarization. Secondly, this wavelength is quite sensitive to Rayleigh scattering within the Venus atmosphere. Thus small variations in the amount of gas or haze particles over the main cloud deck cause a substantial variation in the observed polarization. The range of observed polarization amounts is thus very high at this wavelength leading to a difficulty in detecting small local scale contrasts that we are looking for.

At 365 nm comparatively much greater structure is seen at most phase angles. Sometimes patches of very high polarization show up over the visible disk such about 45 o phase angle. Very little detail is seen at phase angles between 0 and 30o. At higher phase angles the structure seen in the polarization amount is very similar to that seen in the unpolarized intensity data (11e, 11f).

In contrast, the two longer wavelengths show much greater structure and contrast especially at phase angles between 50 and 90 o. However, in some instances, a puzzling lack of detail at these phase angles has been noticed in successive observations on the same orbit. The reasons for this sudden absence of detail are unknown. At 550 nm the signature of the 1.1μ radius cloud particles is also clearly visible as the "cloud bow", a region of very enhanced polarization amount over most of the Venus disk at the 15 to 20o phase angle obervations.

The prominent features in the polarization images are the signature of the cloud-bow near the 18 o phase angle for the 1.1μ radius main cloud layer particles. At other phase angles the visibility of the features is not as high as near 60o phase angle. The remarkable similarity of the shapes and sizes of these polarization features to those seen in the ultraviolet intensity data can be clearly seen.

Frequently the polarization data shows "bow-shaped" features that are often seen in the ultraviolet images of Venus. The resemblence in size and shape of these features is similar that it is indicative of the fact that the same cloud is responsible for both the ultraviolet intensity contrasts and the polarization structure. The 935 nm polarization over the bright arms of the bow shaped features which are bright in the ultraviolet light is negative. This may or may not be consistent with the model proposed by Esposito and Travis (1982) that the bright features in ultraviolet have a greater amount of sub-micron haze over them, the excess optical thickness being 0.1 at 935 nm. According to Kawabata et al. (1980) an optical thickness of about 0.2 at 935 nm is sufficient to produce a significant positive polarization in the polar regions (the index of refraction they used for the haze particles at 935 was 1.46 whereas Esposito and Travis use a value of 1.43 for the sub-micron particles).

Structure has also been observed at times in the direction of polarization data, although to a much lesser degree. It is not known why such variation in the direction of polarization on a local scale is seen only at some times and not at others as well as only at certain phase angles. Figure 11 shows the structure in the direction data seen in observation # 38 at the 365 nm wavelength.

3.5 Movements of the Polarization Features

The fact that discrete isolated features are seen in the polarization data immediately leads to questions such as-- "how long do these features last? Can they be followed from one observation to the next? How do their motions relate to those of the ultraviolet clouds?" etc. Fortunately, the OCPP observations covered several periods when more than one observation was obtained per orbit (see Table I). In some cases four full disk observations were obtained on a single orbit spanning a time period of over 20 hours. It is thus possible to see how the polarization features show up in these consecutive observations.

Figure 12 presents several time sequences of four polarization observations per orbit. The polarization amount has been linearly scaled with the 128 DN representing the zero percent polarization amount. The central meridian in each of the observations is chosen to be the sub-solar meridian. The bow like features seen often in the ultraviolet images show up in the polarization amount at all four wavelengths in several observations and can be easily tracked from one observation to the next.The movement of the polarization features in these observations is from east to west which is in the same sense as the retrograde mean zonal motion determined previously from the movements of the ultraviolet clouds from the OCPP images (Limaye et al. 1982).

The speeds of such features when they can be seen in three or more successive observations is roughly 100 ms^{-1} which is quite comparable to that of the ultraviolet features. Greater accuracy is not possible in these measurements due to the limited spatial resolution of the polarimetry mode observations. The nominal uncertainty is approximately

25 ms^{-1}.

Due to the large variation in the visibility of the polarization features with phase angle as well as the low spatial resolution of the observations, it is not generally possible to track such features in only a pair of observations separated by about 4 to 5 hours, but at least three, and ideally four observations are needed. Unfortunately, the number of such observations obtained at a phase angle of around 60o during the nominal and extended missions is rather limited and thus only a few measurements can be obtained.

Nevertheless a small number of measurements of polarization feature movements were made. It was not possible to compare directly the motions of a given feature in different wavelength as the texture and the visibility of a given feature generally is very different in each wavelength. Thus, comparison of the motions in different wavelengths can only be made though ensemble averages for each wavelength.

Figure 13 presents results of the measurements of the motions of the polarization features at the four wavelengths for the zonal component only. Table III gives a summary of the results in terms of the number of points, RMS deviation etc. The results are averaged in 15o degree latitude bins with the resultant average value of the zonal component of the motions of the features assigned to the average latitude of the observations in that particular bin. In many instances only a single observation was available. It should be emphasized here that these results should be considered as only indicative of the movements of the features and not as definitive results due to the immense difficulty and uncertainties involved.

No consistent differences between the movements of the polarization features in the different wavelengths can be confidently detected except perhaps for 270 nm polarization features which have noticeably faster zonal speeds. However, the confidence in the 270 nm data is low due to the extremely low contrasts visible in the polarization data. In any case the low resolution of the data as well as difficulties in finding features in the different wavelengths make the task a difficult one. If indeed the polarization features are caused mostly by the sub-micron sized haze particles above the main cloud layer, then one would expect somewhat different cloud motions in terms of either the speed or the direction when compared to the motions of the ultraviolet clouds. Simple visual tracking techniques are inadequate for detecting small differences in movements as seen in the different wavelength data and more sophisticated techniques beyond the scope of the present work may prove fruitful in this regard.

These observations show that at least in some instances polarization features (i) persist for periods as long as a day, and (ii) their apparent movements on the disk of Venus are analogous to the movements of the ultraviolet clouds lending credence to the suggestion that they are the signature of some polarizing scatterers that are being carried together as an entity or a cloud mass with the ambient atmospheric flow. Whatever the reasons(s) they appear due to, they must be intimately related to the ultraviolet contrasts considering the similarity in morphology, movements, and lifetimes.

4.0 Summary

The present investigation has shown that there are unmistakable features in the polarization data. The visibility of these features depends on the phase angle and also appears to be time dependent evolution of the cloud/haze mixture. These features last long enough to be tracked over a period as long as a day, enabling them to be used as traces of atmospheric motion. The larger scale features such as the bow-shaped features last longer and can be seen at least four to five days later after they presumably have gone all the way around the planet.

The structure seen in the distribution of the polarization amount over the disk of Venus in all wavelengths is similar to that of the ultraviolet contrasts. However, a given feature need not appear the same in all the wavelengths as could be expected due to the strong dependence of the observed polarization amount on the wavelength. This is also evidenced by the weak but complex phase dependent relationship between the amount of observed polarization and the contrast in the unpolarized intensity at that location in a given wavelength. It is possible that the structure seen in the shorter wavelengths is at a somewhat higher level than that seen in the two longer wavelegths. The results of Esposito and Travis (1982) are significant in this respect in that they suggest that ultraviolet contrasts have differential amounts of the haze material above them.

This relationship between the appearance of the structure in the poalrization data and the ultraviolet contrasts is consistent with the immense time variation seen in the poalrization data if the cloud/haze structure is evolutonary in some regard, i.e. is the haze being created in the brighter (ultraviolet) portions of the clouds, etc ? A detailed monitoring of the structure of the polarization data as a function of time as well as position on the disk of Venus should provide some clues.

An attempt was made to determine the motions of the features in a series of four observations obtained in a succession. Unfortunately the number of such sequences obtained in the early part of the Pioneer Venus mission was too small to allow a more exhaustive effort in determining the movements of these features. No systematic large differences were obvious in the average zonal speeds of the polarization features tracked at the four wavelengths except perhaps the 270 nm features which show somewhat faster speeds, although the low spatial resolution of the polarization data is a serious drawback.

There are many puzzling questions still left to be answered. Foremost of all is the question," why do these polarization features become more visible at moderate phase angles?" What causes them? At what altitude do they correspond to? etc. The analysis of the OCPP images has shown that there are many time variations as well. The ultraviolet clouds are known to be influenced by the atmospheric circulation. What is the influence of the atmospheric circulation on the polarization features?

Some of these questions can be tackled with further analysis. This study represents only an initial step. It is likely that additional data will be available from the Pioneer Venus Orbiter in future. More observations in the polarimetry mode per orbit would enhance the already exisitng data but would allow a better study of the relationships between the ultraviolet contrasts and the overlying haze.

Acknowledgements

I thank Dr. Larry Travis, the Principal Investigator of the OCPP experiment for the use of his data as well as many useful discussions. Thanks are also due to Mr. Lex Lane who inspired a deeper study of the morphology of the polarization features.

Thanks are also due to Drs. Larry Sromovsky and H. Revercomb of the Space Science & Engineering Center for many useful comments.

This work was funded by NASA Grant # NAG 2-93 under the Pioneer Venus Guest Investigator Program.

ORIGINAL PAGE IS
OF POOR QUALITY

References

Colin, L., 1980: The Pioneer Venus missions, J. Geophys. Res., (85), 7375-7598.

Colin, L., and D.M. Hunten, 1977: Pioneer Venus experiment descriptions, Space Sci. Rev., (20), 451-525.

Esposito, L.W., 1980: Ultraviolet contrasts and the absorbers near the Venus cloud tops, J. Geophys. Res., (85), 8151-8157.

Esposito L.W., and L.D. Travis, 1982: Polarization studies of the Venus UV contrasts: CLoud height and haze variability, Icarus, (51), 374-390.

Del Genio, A.D. and W.B. Rossow, 1982: Temporal variability of ultraviolet cloud features in the Venus atmosphere, Icarus, (51), 391-415.

Kawabata, K., D.L. Coffeen, J.E. Hansen, W.A. Lane, M. Sato, and L.D. Travis, 1980: Cloud and haze properties from Pioneer Venus polarimetry, J. Geophys. Res. , (85), 8129-8140.

Kawabata, K., 1981: Investigation of some of the principal geometric effects on planetary polarization, The Moon and the Planets, (24), 291-318.

Limaye, S.S., and V.E. Suomi, 1977: A normalized view of Venus, J. Atmos. Sci., (34), 205-215.

Limaye, S.S., 1982a: Morphology of polarization features on Venus, Abstract of paper presented at the fourth annual meeting of Planetary Atmospheres Principal Investigators, April 21-23, S.K. Atreya and D.A. Swartz, Ed., University of Michigan, Ann Arbor, Michigan.

Limaye, S.S., 1982b: Polarization Features on Venus, Abstract of paper presented at the Fourteenth ANnual Meeting of the Division of Planetary Sciences, Boulder, Colorado, October 19-22 ,Bull. Amer. Astron. Soc., (14), 740.

Limaye, S.S., C.J. Grund, and S.P. Burre, 1982: Zonal mean circulation at the cloud level on Venus: Spring and Fall 1979 OCPP observations, Icarus, (51), 416-439.

Limaye, S.S., 1983: Polarization features on Venus, Submitted to Icarus.

Lyot, B., 1929: Recherches sur la polarisation de la lumier des planetes et de quelques substances terrestres, Ann. Obs. Paris (Meudon), (8).

Russel, E., L. Watts, S. Pellicori, and D. Coffeen, 1977: Orbiter cloud photopolarimeter for the Pioneer Venus mission, Proc. Soc. Photo. Opt.

Instrum. Eng., (112), 28-44.

Travis, L.D., 1975: On the origin of the ultraviolet contrasts on Venus, J. Atmos. Sci., (32), 1190-1200.

Travis, L.D., D.L. Coffeen, J.E. Hansen, K. Kawabata, A.A. Lacis, W.A. Lane, S.S. Limaye, P.H. Stone, 1979: Orbiter Cloud Photopolarimeter investigation, Science, (203), 781-785.

Travis, L.D., D.L. Coffeen, A.D. Del Genio, J.E. Hansen, K. Kawabata, A.A. Lacis, W.A. Lane, S.S. Limaye, W.B. Rossow, and P.H. Stone, 1979: Cloud images from the Pioneer Venus orbiter, Science, (205), 74-76.

Figure Captions

Figure 1. Phase angle variation for the polarimetry observations obtained from the OCPP instrument.

Figure 2. An example of a composite view of the linearly and logarithmically scaled polarization amount in the rectangular and polar projections as well of the unpolarized intensity and the direction of polarization, for 270 (a), 365 (b), 550 (c), and 935 nm (d) data. The top row represents the linearly scaled polarization amount, the left most image representing the rectangular map about the sub-spacecraft meridian while the two images on the right represent respectively the northern and the southern hemisperes in polar stereographic projection. The middle row has the same format as the top row except that it represents the unpolarized intensity. The positive and negative polarization amounts scaled logarithmically are shown in the two left most images in the bottom row in a rectangular map similar to that for the linearly scaled polarization and intensity data. The right most image in the bottom row represents the variation of the direction of polarization.

Figure 3. Minnaert plots showing the relationship between I/μ and $\mu\mu_o$ on a logarithmic scale for observations taken at 4.0 (a), 11.89 (b), 28.6 (c), 42.8 (d), 51.8 (e), 62.9 (f), 88.5 (g), and 99.0o (h). The least squares fit to the data for each wavelength are also shown. The

resultant values of the intercept and slopes for the fitted lines are indicated on the top in each figure.

Figure 4. Variation of a_o, the intercept value from Minnaert fit, as a function of phase angle. This represents the intensity observed at normal viewing angle for the case of normal incidence (i.e. when both μ and μ_o = 1), and is hence proportional to the "normal albedo". The values of a_o beyond about 100^o phase angle may be unreliable.

Figure 5. Variation of the coefficient of determination of the least squares solution to the observed data shown in Figure 3. The linear coefficient of correlation between $\ln(I/\mu)$ and $\ln(\mu\mu_o)$ is the square root of the coefficient of determination. As can be seen the Minnaert fit is very poor beyond 100^o phase angle.

Figure 6. Variation of k, the limb darkening coefficient, or the slope of the least square fit line (Figure 3) as a function of phase angle. Comments regarding variation a_o apply in this case as well.

Figure 7. Variation of contrast defined as the absolute deviation from the Minnaert law intensity variation (a), and the corresponding root mean square value (b).

Figure 8. Variation of the coefficient of correlation between (a) observed polarization amount and the contrast as a function of phase

angle, and, (b) dependence of the coefficient of correlation between the observed polarization amount and the direction of polarization, on the phase angle.

Figure 9. Variation of disk integrated absolute polarization amount (a), the direction of polarization (b), and the observed intensity (c).

Figure 10. Montage of selected polarization images at 270 (a), 365 (b), 550 (c), and 935 nm (d), and unpolarized intensity images at 270 (e) and 365 nm (f). Observations are presented at roughly 5o phase angle interval. Table II gives the relevent information about the specific observations shown.

Figure 11. An example of structure seen in the variation of direction of polarization over the disk. This observation (#138) was obtained at 365 nm.

Figure 12. Time series of polarimetry observations obtained on a orbits 44 (a), 80 (b), 333/334 (c), 336/337 (d), 337/338 (e), and 339/340 (f). From left to right the images represent the 270, 365, 550 and 935 nm polarization amount (positive and negative, linearly scaled with 128 DN representing the zero percent level), and the 365 nm intensity, all in rectangular projection. The first row represents the first observation in a sequence and subsequent observations are presented in successive rows. The nominal time interval between the first observation and the

next one on the same orbit is between 4 and 5 hours.

Figure 13. Average zonal speed of the movements of polarization features for each wavelength as indicated by the different curves. These results were obtained by tracking polarization features in successive observations (Figure 12) in each wavelength, and then averaging the zonal components obtained in 15° wide latitude bins.

ORIGINAL PAGE IS
OF POOR QUALITY

Table I. OCPP Polarimetry Observations used in this study. SCLAT and SCLON refer to sub-spacecraft point on Venus, while SSLAT and SSLON refer to the sub-solar point on Venus. All quantities refer to the center of Venus, i.e. when the OCPP optic axis passes through the Venus center during a particular observation.

Map#	Orb#	Date	DOY	HH:MM:SS	Phase	Range	Celestial			
					(Deg)	(Km)	SCLAT	SCLON	SSLAT	SSLON
0005	0004	8 DEC 1978	342	20:10:05	112.9	51435.4	-35.8	34.1	-1.1	-85.5
0009	0006	10 DEC 1978	344	17:48:42	110.1	34092.8	-48.9	40.8	-1.2	-82.4
0010	0006	10 DEC 1978	344	21:58:47	109.9	58138.5	-30.8	32.0	-1.3	-82.1
0011	0007	11 DEC 1978	345	03:37:19	107.9	66802.5	-17.0	27.5	-1.3	-81.7
0012	0007	11 DEC 1978	345	12:17:20	100.4	33463.2	13.2	19.3	-1.3	-81.1
0014	0008	12 DEC 1978	346	22:18:24	107.1	58418.0	-30.6	32.0	-1.4	-78.8
0015	0009	13 DEC 1978	347	04:01:05	104.8	66739.6	-16.7	27.4	-1.5	-78.5
0016	0009	13 DEC 1978	347	12:36:43	97.1	32936.4	13.5	19.1	-1.5	-77.9
0020	0010	14 DEC 1978	348	12:49:57	95.4	32421.9	14.0	19.0	-1.6	-76.2
0021	0010	14 DEC 1978	348	18:31:13	105.8	35594.3	-47.5	39.9	-1.6	-75.9
0022	0010	14 DEC 1978	348	22:47:01	104.1	59147.8	-30.0	31.8	-1.6	-75.6
0026	0011	15 DEC 1978	349	23:05:42	102.6	59618.5	-29.7	31.7	-1.7	-73.9
0036	0030	4 JAN 1979	004	06:02:31	70.9	66865.4	-19.2	28.2	-3.0	-42.6
0038	0032	6 JAN 1979	006	06:16:13	67.8	66823.2	-19.0	28.2	-3.1	-39.3
0039	0033	7 JAN 1979	007	06:22:06	66.2	66824.5	-19.0	28.2	-3.1	-37.7
0041	0035	9 JAN 1979	009	06:32:48	63.1	66817.3	-19.0	28.2	-3.2	-34.4
0042	0040	13 JAN 1979	013	22:10:29	72.1	35957.1	-47.2	40.2	-3.3	-26.9
0056	0043	16 JAN 1979	016	16:19:00	44.2	35189.5	11.3	19.5	-3.4	-22.4
0060	0044	17 JAN 1979	017	12:38:16	45.1	56996.4	-5.2	24.1	-3.4	-21.0
0061	0044	17 JAN 1979	017	16:22:34	42.6	35253.5	11.2	19.5	-3.4	-20.8
0062	0044	17 JAN 1979	017	22:27:14	67.9	35914.4	-47.1	40.3	-3.4	-20.4
0065	0045	18 JAN 1979	018	12:43:33	43.4	56933.5	-5.2	24.1	-3.4	-19.4
0066	0045	18 JAN 1979	018	16:25:50	41.1	35425.7	11.1	19.5	-3.4	-19.2
0067	0046	19 JAN 1979	019	14:51:53	40.0	46841.2	2.3	22.0	-3.4	-17.6
0069	0048	21 JAN 1979	021	10:41:21	40.9	63501.9	-11.2	25.8	-3.4	-14.7
0071	0050	23 JAN 1979	023	10:46:50	37.8	63568.6	-11.3	25.9	-3.4	-11.4
0073	0052	25 JAN 1979	025	11:00:37	34.4	63272.0	-10.9	25.7	-3.4	-8.2
0074	0053	26 JAN 1979	026	11:03:29	32.9	63238.2	-10.9	25.7	-3.4	-6.5
0082	0059	2 FEB 1979	033	07:29:07	28.6	66564.1	-19.7	28.5	-3.2	4.6
0083	0060	2 FEB 1979	033	23:03:23	53.9	34925.8	-47.6	41.1	-3.2	5.6
0084	0060	3 FEB 1979	034	02:45:50	38.1	56683.9	-31.6	32.8	-3.2	5.9
0085	0061	3 FEB 1979	034	13:59:34	16.8	54411.9	-3.2	23.4	-3.2	6.6
0088	0061	4 FEB 1979	035	02:46:04	37.2	56678.8	-31.6	32.8	-3.2	7.5
0089	0062	4 FEB 1979	035	13:59:49	15.2	54486.8	-3.2	23.4	-3.1	8.2
0093	0063	6 FEB 1979	037	02:46:57	35.4	56576.5	-31.7	32.9	-3.1	10.7
0094	0064	6 FEB 1979	037	14:00:05	11.9	54502.4	-3.2	23.4	-3.1	11.5
0097	0064	7 FEB 1979	038	02:47:07	34.6	56576.3	-31.7	32.9	-3.0	12.3
0104	0069	11 FEB 1979	042	13:55:31	4.0	54807.3	-3.4	23.5	-2.8	19.5

Table I (continued)

Map#	Orb#	Date	DOY	HH:MM:SS	Phase (Deg)	Range (Km)	Celestial SCLAT	SCLON	SSLAT	SSLON
0110	0071	13 FEB 1979	044	13:52:08	1.1	54973.6	-3.5	23.5	-2.7	22.7
0116	0073	15 FEB 1979	046	13:43:56	2.7	55478.5	-3.9	23.6	-2.6	25.9
0124	0079	21 FEB 1979	052	22:46:54	46.1	33826.2	-48.0	41.6	-2.2	36.2
0126	0080	22 FEB 1979	053	13:33:00	13.7	55344.6	-3.6	23.5	-2.1	37.2
0127	0080	22 FEB 1979	053	17:05:49	24.0	33623.7	13.0	18.6	-2.1	37.4
0128	0080	22 FEB 1979	053	22:45:28	46.0	34025.7	-48.0	41.5	-2.1	37.8
0129	0080	23 FEB 1979	054	02:20:14	30.2	55754.2	-32.0	33.0	-2.1	38.0
0132	0081	23 FEB 1979	054	22:42:48	46.0	33973.1	-48.0	41.5	-2.0	39.4
0134	0082	24 FEB 1979	055	13:30:12	16.9	55183.9	-3.5	23.5	-2.0	40.4
0136	0083	25 FEB 1979	056	13:25:03	18.5	55375.1	-3.6	23.5	-1.9	42.0
0138	0083	25 FEB 1979	056	22:37:17	46.2	33968.3	-48.0	41.5	-1.9	42.6
0139	0083	26 FEB 1979	057	02:09:57	31.6	55503.6	-32.1	33.1	-1.9	42.8
0140	0084	26 FEB 1979	057	13:21:27	20.1	55444.8	-3.7	23.6	-1.8	43.6
0143	0084	27 FEB 1979	058	02:04:11	32.3	55332.9	-32.2	33.1	-1.8	44.4
0144	0085	27 FEB 1979	058	13:16:36	21.6	55593.1	-3.8	23.6	-1.7	45.2
0147	0086	28 FEB 1979	059	23:56:54	39.4	44747.7	-39.8	36.5	-1.6	47.5
0149	0087	1 MAR 1979	060	23:53:40	39.8	44819.0	-39.7	36.5	-1.5	49.1
0153	0089	3 MAR 1979	062	23:56:11	40.4	45800.8	-39.0	36.1	-1.4	52.3
0155	0090	4 MAR 1979	063	23:52:39	41.1	45762.9	-39.0	36.1	-1.3	53.9
0157	0091	5 MAR 1979	064	23:46:07	41.9	45501.3	-39.2	36.2	-1.2	55.4
0161	0093	7 MAR 1979	066	23:37:20	43.4	45288.3	-39.4	36.2	-1.0	58.6
0163	0094	8 MAR 1979	067	23:24:48	44.6	44323.1	-40.0	36.5	-0.9	60.2
0165	0094	9 MAR 1979	068	04:47:04	37.4	64653.1	-23.3	29.7	-0.9	60.6
0166	0095	9 MAR 1979	068	15:03:41	40.7	43031.8	5.6	21.0	-0.9	61.2
0169	0097	11 MAR 1979	070	14:52:39	43.7	43453.1	5.3	21.1	-0.7	64.4
0172	0100	14 MAR 1979	073	15:01:32	48.8	42068.9	6.5	20.8	-0.4	69.2
0175	0101	15 MAR 1979	074	10:46:55	45.9	61902.0	-8.7	25.2	-0.3	70.5
0176	0101	15 MAR 1979	074	15:04:58	50.2	42391.2	6.3	20.9	-0.3	70.8
0177	0102	16 MAR 1979	075	14:15:43	50.3	47974.5	2.2	22.1	-0.2	72.3
0178	0104	18 MAR 1979	077	09:53:21	50.2	64397.6	-11.5	26.0	-0.1	75.2
0180	0107	21 MAR 1979	080	14:18:59	57.8	49859.3	0.9	22.5	0.2	80.3
0181	0109	23 MAR 1979	082	14:49:18	61.4	47842.3	2.3	22.1	0.4	83.5
0185	0113	27 MAR 1979	086	14:57:02	67.5	48740.9	1.7	22.3	0.8	89.8
0188	0117	31 MAR 1979	090	15:26:45	74.0	47705.9	2.4	22.2	1.2	96.2
0191	0121	4 APR 1979	094	15:50:06	80.4	47010.3	3.0	22.1	1.5	102.5
0192	0126	9 APR 1979	099	16:15:00	88.3	46579.3	3.2	22.0	1.9	110.5
0194	0129	12 APR 1979	102	16:22:14	93.0	47050.9	2.9	22.1	2.1	115.2
0196	0130	13 APR 1979	103	16:24:30	94.5	47248.1	2.7	22.2	2.2	116.8
0199	0133	16 APR 1979	106	16:32:02	99.2	47518.5	2.5	22.2	2.4	121.5
0201	0135	18 APR 1979	108	16:44:33	102.4	46965.0	2.6	22.2	2.5	124.7
0202	0137	20 APR 1979	110	16:49:56	105.6	47006.1	2.8	22.1	2.7	127.9

ORIGINAL PAGE IS
OF POOR QUALITY

Table I (continued)

Map#	Orb#	Date	DOY	HH:MM:SS	Phase (Deg)	Range (Km)	Celestial SCLAT	SCLON	SSLAT	SSLON
0203	0138	21 APR 1979	111	16:52:39	107.2	46995.5	2.8	22.1	2.7	129.5
0204	0141	24 APR 1979	114	17:02:02	111.9	46740.6	3.0	22.1	2.9	134.2
0205	0142	25 APR 1979	115	17:16:28	113.7	45564.7	3.8	21.8	2.9	135.8
0206	0144	27 APR 1979	117	17:28:06	117.0	44643.1	4.5	21.6	3.0	139.0
0214	0173	27 MAY 1979	147	01:48:02	137.6	49725.0	-36.0	34.8	3.2	-174.4
0215	0173	27 MAY 1979	147	06:28:18	150.1	64889.8	-22.6	29.4	3.2	-174.1
0218	0174	27 MAY 1979	147	23:48:24	129.5	37396.9	-45.0	39.3	3.2	-173.0
0219	0174	28 MAY 1979	148	03:49:05	145.2	58842.2	-29.1	31.7	3.2	-172.7
0220	0175	28 MAY 1979	148	08:42:26	155.9	66380.0	-17.1	27.6	3.2	-172.4
0223	0175	29 MAY 1979	149	02:01:07	140.8	51901.5	-34.4	34.1	3.1	-171.2
0231	0177	31 MAY 1979	151	03:16:28	147.3	58102.4	-29.6	32.2	3.1	-168.0
0232	0177	31 MAY 1979	151	08:06:46	158.8	66351.5	-17.7	27.9	3.0	-167.6
0237	0178	1 JUN 1979	152	01:23:05	142.3	50601.5	-35.3	34.6	3.0	-166.5
0241	0179	2 JUN 1979	153	01:36:23	143.2	51112.7	-35.1	34.5	3.0	-164.9
0242	0180	3 JUN 1979	154	01:39:31	143.5	50653.5	-35.4	34.6	2.9	-163.3
0243	0181	4 JUN 1979	155	06:11:03	157.2	65067.5	-22.9	29.7	2.9	-161.4
0244	0182	5 JUN 1979	156	01:47:31	144.1	49933.1	-35.9	34.8	2.8	-160.1
0245	0182	5 JUN 1979	156	06:19:11	157.9	65063.9	-22.9	29.7	2.8	-159.8
0246	0225	17 JUL 1979	198	17:25:44	113.6	47577.3	3.1	22.0	-0.7	-91.6
0248	0226	18 JUL 1979	199	17:22:32	112.1	47811.3	2.9	22.1	-0.8	-90.0
0261	0238	30 JUL 1979	211	17:28:35	92.8	47562.9	3.1	22.1	-1.9	-70.6
0262	0241	2 AUG 1979	214	17:52:45	87.6	45524.3	4.6	21.7	-2.1	-65.7
0269	0246	7 AUG 1979	219	17:07:29	80.4	50308.1	1.1	22.7	-2.5	-57.6
0303	0292	23 SEP 1979	266	04:44:09	37.6	47773.2	-36.8	35.4	-2.9	17.8
0304	0293	24 SEP 1979	267	04:53:10	37.0	47734.9	-36.8	35.4	-2.8	19.4
0305	0294	25 SEP 1979	268	05:03:58	36.5	47798.7	-36.8	35.4	-2.8	21.0
0313	0303	3 OCT 1979	276	14:10:36	14.7	66733.0	-15.1	27.2	-2.3	34.5
0422	0310	11 OCT 1979	284	11:14:03	27.7	63611.9	-23.9	30.1	-1.6	47.1
0425	0311	12 OCT 1979	285	11:19:21	28.7	63559.3	-23.9	30.1	-1.6	48.7
0428	0312	13 OCT 1979	286	11:23:42	29.8	63468.5	-24.0	30.1	-1.5	50.3
0431	0313	14 OCT 1979	287	11:31:58	30.9	63530.1	-23.9	30.1	-1.4	51.9
0434	0314	15 OCT 1979	288	11:32:36	32.1	63336.2	-24.1	30.2	-1.3	53.5

ORIGINAL PAGE IS
OF POOR QUALITY

Table I (continued)

Map#	Orb#	Date	DOY	HH:MM:SS	Phase (Deg)	Range (Km)	Celestial SCLAT	SCLON	SSLAT	SSLON
0437	0315	16 OCT 1979	289	11:35:29	33.3	63203.2	-24.3	30.2	-1.2	55.1
0440	0316	17 OCT 1979	290	11:30:04	34.6	63081.4	-24.4	30.3	-1.1	56.7
0445	0318	19 OCT 1979	292	10:06:42	38.7	57888.6	-29.1	32.0	-1.0	59.8
0451	0320	21 OCT 1979	294	10:45:31	40.5	59440.4	-27.8	31.5	-0.8	63.0
0453	0321	22 OCT 1979	295	09:47:21	42.8	55413.9	-31.0	32.6	-0.7	64.6
0469	0324	24 OCT 1979	297	22:51:07	46.8	48396.2	3.2	21.9	-0.4	68.6
0492	0329	30 OCT 1979	303	13:24:23	51.8	63985.6	-23.3	29.8	0.1	77.5
0495	0333	2 NOV 1979	306	23:58:55	61.2	47215.2	4.1	21.8	0.4	83.0
0496	0333	3 NOV 1979	307	09:44:27	58.2	49304.3	-35.3	34.3	0.4	83.6
0497	0333	3 NOV 1979	307	14:31:02	57.7	65242.9	-21.5	29.2	0.5	83.9
0498	0334	3 NOV 1979	307	19:41:10	59.2	63895.9	-9.5	25.6	0.5	84.3
0499	0334	4 NOV 1979	308	00:01:33	62.7	47524.9	3.9	21.8	0.5	84.5
0500	0334	4 NOV 1979	308	09:51:47	59.4	49400.9	-35.3	34.3	0.5	85.2
0501	0334	4 NOV 1979	308	14:32:52	59.1	65118.9	-21.7	29.3	0.6	85.5
0502	0335	5 NOV 1979	309	09:55:35	60.7	49208.9	-35.4	34.3	0.6	86.8
0503	0336	6 NOV 1979	310	09:58:29	61.9	48918.3	-35.6	34.4	0.7	88.4
0504	0336	6 NOV 1979	310	14:33:24	62.1	64827.0	-22.2	29.4	0.7	88.7
0505	0337	6 NOV 1979	310	19:44:21	63.8	64383.0	-10.1	25.8	0.8	89.0
0506	0337	7 NOV 1979	311	00:09:12	67.2	48458.0	3.2	22.1	0.8	89.3
0507	0337	7 NOV 1979	311	10:01:51	63.2	48657.3	-35.8	34.4	0.8	90.0
0508	0337	7 NOV 1979	311	14:34:42	63.5	64687.7	-22.4	29.5	0.8	90.3
0509	0338	7 NOV 1979	311	19:43:58	65.3	64596.2	-10.4	25.9	0.8	90.6
0510	0338	8 NOV 1979	312	00:12:22	68.8	48725.3	3.0	22.1	0.9	90.9
0511	0338	8 NOV 1979	312	10:04:06	64.5	48395.3	-36.0	34.5	0.9	91.5
0512	0338	8 NOV 1979	312	14:36:17	65.0	64566.5	-22.5	29.5	0.9	91.8
0513	0339	8 NOV 1979	312	19:45:29	66.9	64710.9	-10.6	25.9	0.9	92.2
0514	0339	9 NOV 1979	313	00:15:01	70.3	49020.4	2.8	22.2	1.0	92.5
0515	0339	9 NOV 1979	313	10:07:49	65.7	48095.7	-36.2	34.6	1.0	93.1
0516	0339	9 NOV 1979	313	14:35:44	66.4	64353.2	-22.8	29.6	1.0	93.4
0517	0340	9 NOV 1979	313	19:45:51	68.4	64879.2	-10.8	26.0	1.0	93.8
0518	0340	10 NOV 1979	314	00:17:58	71.3	49375.0	2.6	22.3	1.0	94.1
0521	0341	11 NOV 1979	315	00:21:34	73.3	49562.7	2.4	22.3	1.1	95.6
0523	0342	11 NOV 1979	315	19:49:26	71.5	65075.4	-11.1	26.1	1.2	96.9
0524	0342	12 NOV 1979	316	00:24:38	74.8	49783.2	2.2	22.4	1.2	97.2
0527	0343	13 NOV 1979	317	00:26:46	76.3	50159.0	2.0	22.5	1.3	98.8
0530	0344	14 NOV 1979	318	00:30:45	77.9	50279.7	1.9	22.5	1.4	100.4
0542	0349	19 NOV 1979	323	01:32:55	86.4	47109.1	4.1	21.9	1.8	108.4

ORIGINAL PAGE IS
OF POOR QUALITY

Table I (continued)

Map#	Orb#	Date	DOY	HH:MM:SS	Phase (Deg)	Range (Km)	Celestial SCLAT	SCLON	SSLAT	SSLON
0545	0350	20 NOV 1979	324	01:34:18	87.9	47396.9	3.9	22.0	1.9	110.0
0548	0351	21 NOV 1979	325	01:45:07	89.5	46848.6	4.3	21.9	2.0	111.6
0550	0352	22 NOV 1979	326	01:47:27	91.1	47159.3	4.1	21.9	2.0	113.1
0551	0354	23 NOV 1979	327	21:36:21	90.7	63816.5	-9.5	25.7	2.2	116.0
0558	0360	30 NOV 1979	334	02:25:52	103.7	47057.6	4.1	21.9	2.6	125.8
0559	0361	30 NOV 1979	334	22:08:39	101.7	63746.0	-9.5	25.7	2.6	127.1
0560	0361	1 DEC 1979	335	02:26:33	105.2	47355.9	3.9	22.0	2.6	127.4
0561	0362	1 DEC 1979	335	22:12:50	103.3	63722.1	-9.5	25.7	2.7	128.7
0562	0362	2 DEC 1979	336	02:27:14	106.7	47571.6	3.7	22.0	2.7	129.0
0563	0364	3 DEC 1979	337	22:21:09	106.5	63622.3	-9.4	25.6	2.8	131.9
0570	0366	6 DEC 1979	340	02:39:37	113.0	47626.9	3.6	22.0	2.9	135.3
0572	0367	7 DEC 1979	341	02:41:25	114.6	47703.6	3.6	22.0	3.0	136.9
0573	0368	7 DEC 1979	341	22:20:21	112.6	64019.5	-9.9	25.8	3.0	138.2
0574	0368	8 DEC 1979	342	02:43:12	116.2	47759.9	3.5	22.0	3.0	138.5
0575	0369	8 DEC 1979	342	22:22:08	114.2	64036.5	-10.0	25.8	3.0	139.8
0576	0369	9 DEC 1979	343	02:45:02	117.7	47818.8	3.5	22.1	3.0	140.1
0577	0370	9 DEC 1979	343	22:22:13	115.7	64107.5	-10.1	25.8	3.1	141.4
0578	0370	10 DEC 1979	344	02:45:56	119.3	48040.4	3.3	22.1	3.1	141.7
0579	0371	10 DEC 1979	344	22:21:56	117.2	64212.1	-10.2	25.9	3.1	143.0
0580	0371	11 DEC 1979	345	02:46:40	120.8	48165.1	3.2	22.1	3.1	143.3
0581	0394	2 JAN 1980	002	22:28:20	153.5	63289.2	-9.2	25.5	3.3	179.5
0583	0394	3 JAN 1980	003	11:21:14	130.7	42610.7	-39.9	36.9	3.3	-179.7
0584	0394	3 JAN 1980	003	15:11:33	142.7	60550.5	-26.5	31.1	3.3	-179.4
0587	0395	4 JAN 1980	004	04:19:15	156.1	35089.2	13.3	18.8	3.3	-178.6
0588	0395	4 JAN 1980	004	11:08:02	130.9	41494.8	-40.7	37.3	3.3	-178.1
0589	0395	4 JAN 1980	004	14:53:12	143.3	59802.5	-27.1	31.4	3.3	-177.9
0590	0396	4 JAN 1980	004	19:52:19	152.9	66368.1	-15.1	27.3	3.3	-177.5
0592	0396	5 JAN 1980	005	04:16:17	157.2	34973.0	13.4	18.8	3.2	-177.0
0597	0397	6 JAN 1980	006	04:12:35	158.2	34898.5	13.5	18.7	3.2	-175.4
0599	0397	6 JAN 1980	006	14:48:24	145.7	59985.7	-26.9	31.3	3.2	-174.7
0604	0398	7 JAN 1980	007	14:43:01	146.7	59961.2	-26.9	31.3	3.2	-173.1
0607	0399	8 JAN 1980	008	04:02:35	160.1	34945.6	13.5	18.7	3.2	-172.2
0608	0399	8 JAN 1980	008	10:50:35	134.3	41517.4	-40.6	37.3	3.1	-171.8
0609	0399	8 JAN 1980	008	14:35:29	147.6	59794.8	-27.0	31.4	3.1	-171.5
0610	0400	8 JAN 1980	008	19:33:29	158.3	66324.5	-15.0	27.3	3.1	-171.2
0612	0400	9 JAN 1980	009	03:55:53	161.1	35152.4	13.3	18.7	3.1	-170.6
0613	0400	9 JAN 1980	009	10:45:04	135.1	41578.2	-40.5	37.3	3.1	-170.2
0614	0400	9 JAN 1980	009	14:30:10	148.6	59876.7	-27.0	31.4	3.1	-169.9
0617	0401	10 JAN 1980	010	10:52:47	135.9	41715.4	-40.5	37.3	3.1	-168.6
0618	0401	10 JAN 1980	010	14:39:52	149.6	60153.7	-26.9	31.3	3.1	-168.3

ORIGINAL PAGE IS
OF POOR QUALITY

Table I (continued)

Map#	Orb#	Date	DOY	HH:MM:SS	Phase (Deg)	Range (Km)	Celestial SCLAT	SCLON	SSLAT	SSLON
0619	0402	10 JAN 1980	010	19:41:11	166.[illegible]	[illegible]4731.2	-14.9	27.2	3.1	-168.0
0625	0403	12 JAN 1980	012	17:53:27	158.9	66207.1	-19.4	28.7	3.0	-164.9
0626	0404	13 JAN 1980	013	12:19:23	143.4	48932.8	-35.3	34.8	2.9	-163.7
0627	0404	13 JAN 1980	013	16:41:53	156.7	64418.8	-22.4	29.7	2.9	-163.4
0628	0405	14 JAN 1980	014	12:24:24	143.9	48862.6	-35.4	34.8	2.9	-162.1
0632	0407	16 JAN 1980	016	12:37:46	145.3	49035.0	-35.1	34.7	2.8	-158.9
0635	0408	17 JAN 1980	017	12:36:45	145.4	48539.0	-35.5	34.9	2.7	-157.3
0636	0408	17 JAN 1980	017	17:11:49	159.7	64651.6	-22.0	29.6	2.7	-157.0
0638	0409	18 JAN 1980	018	12:41:38	145.9	48631.3	-35.4	34.9	2.7	-155.7
0645	0422	31 JAN 1980	031	03:02:39	157.0	49536.4	2.7	21.9	1.8	-135.5
0648	0424	1 FEB 1980	032	22:44:58	156.9	64333.2	-9.9	25.7	1.6	-132.[illegible]
0649	0424	2 FEB 1980	033	03:04:51	153.8	49205.9	3.0	21.9	1.6	-132.3
0650	0425	2 FEB 1980	033	22:49:14	155.4	64140.1	-9.6	25.6	1.6	-13[illegible].0
0651	0425	3 FEB 1980	034	03:06:49	152.1	48927.6	3.2	21.8	1.5	-130.7
0652	0426	3 FEB 1980	034	22:54:08	153.8	63939.4	-9.4	25.5	1.5	-129.4
0653	0426	4 FEB 1980	035	03:09:33	150.5	48545.4	3.5	21.7	1.5	-129.1
0656	0428	5 FEB 1980	036	22:57:09	150.7	6[illegible]756.8	-9.1	25.5	1.3	-126.2
0660	0430	8 FEB 1980	039	02:50:36	144.8	50941.8	1.9	22.2	1.1	-122.7
0664	0432	10 FEB 1980	041	03:02:05	141.6	50748.5	2.1	22.2	0.9	-119.5
0666	0433	11 FEB 1980	042	03:08:11	140.0	50616.8	2.2	22.2	0.8	-117.9
0668	0434	12 FEB 1980	043	03:13:32	138.4	50613.5	2.2	22.2	0.7	-116.3
0672	04[illegible]	14 FEB 1980	045	23:27:09	136.6	64267.7	-9.4	25.6	0.5	-111.7
0673	0437	15 FEB 1980	046	03:31:07	133.5	50166.8	2.6	22.1	0.4	-111.4
0676	0439	16 FEB 1980	047	23:39:59	133.4	64164.8	-9.3	25.6	0.3	-108.5
0677	0439	17 FEB 1980	048	03:42:27	130.2	49974.2	2.7	22.1	0.3	-108.2
0678	0440	17 FEB 1980	048	23:46:25	131.7	64071.6	-9.2	25.5	0.2	-106.8
0679	0440	18 FEB 1980	049	03:48:09	128.6	49811.8	2.9	22.1	0.2	-106.6
0683	0442	20 FEB 1980	051	03:59:21	125.4	49585.4	3.0	22.1	-0.0	-103.3
0685	0459	8 MAR 1980	068	13:51:53	105.3	41[illegible]64.2	-40.6	36.6	-1.6	-75.2
0686	0459	8 MAR 1980	068	18:00:29	103.2	60986.6	-25.7	30.6	-1.6	-74.9
0687	0460	8 MAR 1980	068	23:07:03	100.7	66411.7	-13.5	26.8	-1.7	-74.6
0688	0460	9 MAR 1980	069	03:44:52	97.7	55623.1	-1.4	23.5	-1.7	-74.3
0690	0460	9 MAR [illegible]80	069	13:48:22	104.1	40536.6	-41.0	36.8	-1.7	-73.6
0691	0460	9 MAR 1980	069	18:06:58	101.7	61153.3	-25.5	30.6	-1.7	-73.3
0693	0461	10 MAR 1980	070	03:50:33	96.0	55368.7	-1.3	23.4	-1.8	-72.6
0694	0461	10 MAR 1980	070	07:21:13	91.6	33714.7	15.3	18.8	-1.8	-72.4
0695	0461	10 MAR 1980	070	13:54:38	102.8	40956.4	-40.7	36.7	-1.8	-72.0
0696	0461	10 MAR 1980	070	18:14:57	100.2	61398.5	-25.3	30.5	-1.8	-71.7
0697	0462	10 MAR 1980	070	23:20:43	97.4	66306.2	-13.2	26.8	-1.8	-71.3
0698	0462	11 MAR 1980	071	03:57:08	94.3	55038.9	-1.0	23.4	-1.8	-71.0

ORIGINAL PAGE IS
OF POOR QUALITY

Table I (continued)

Map#	Orb#	Date	DOY	HH:MM:SS	Phase (Deg)	Range (Km)	Celestial SCLAT	SCLON	SSLAT	SSLON
0699	0462	11 MAR 1980	071	07:23:09	90.1	33755.6	15.3	18.8	-1.9	-70.8
0700	0462	11 MAR 1980	071	13:59:26	101.5	41247.0	-40.5	36.6	-1.9	-70.3
0701	0462	11 MAR 1980	071	18:21:03	98.6	61605.9	-25.1	30.4	-1.9	-70.0
0703	0463	12 MAR 1980	072	03:59:40	92.7	55083.5	-1.1	23.4	-1.9	-69.4
0704	0463	12 MAR 1980	072	07:27:01	88.5	33543.4	15.5	18.8	-1.9	-69.1
0705	0463	12 MAR 1980	072	15:37:28	99.0	50892.5	-33.6	33.5	-2.0	-68.6
0706	0463	12 MAR 1980	072	20:16:20	96.1	65396.5	-20.5	28.9	-2.0	-68.3
0707	0464	13 MAR 1980	073	01:24:17	93.0	63413.6	-8.5	25.4	-2.0	-67.9
0708	0464	13 MAR 1980	073	05:38:12	89.6	46902.8	4.9	21.8	-2.0	-67.6
0713	0466	15 MAR 1980	075	15:08:24	95.3	47661.0	-35.9	34.4	-2.2	-63.8
0715	0467	16 MAR 1980	076	15:12:45	94.0	47897.3	-35.7	34.4	-2.3	-62.1
0716	0467	16 MAR 1980	076	19:43:40	90.3	64297.5	-22.1	29.5	-2.3	-61.8
0717	0468	17 MAR 1980	077	15:15:13	92.6	47964.0	-35.7	34.4	-2.3	-60.5
0718	0468	17 MAR 1980	077	19:48:39	88.8	64391.8	-22.0	29.4	-2.3	-60.2
0719	0469	18 MAR 1980	078	15:17:50	91.2	47996.2	-35.7	34.4	-2.4	-58.9
0720	0469	18 MAR 1980	078	19:49:59	87.3	64369.1	-22.0	29.4	-2.4	-58.6
0721	0470	19 MAR 1980	079	15:19:24	89.9	48029.3	-35.6	34.4	-2.5	-57.3
0722	0470	19 MAR 1980	079	19:52:40	85.7	64399.7	-22.0	29.4	-2.5	-56.9
0724	0471	20 MAR 1980	080	05:32:00	78.6	48749.3	3.5	22.2	-2.5	-56.3
0728	0472	21 MAR 1980	081	19:58:04	82.6	64470.4	-21.9	29.4	-2.6	-53.7
0729	0473	22 MAR 1980	082	15:25:59	85.8	48093.5	-35.6	34.4	-2.7	-52.4
0730	0473	22 MAR 1980	082	20:00:59	81.1	64479.0	-21.9	29.4	-2.7	-52.1
0731	0478	27 MAR 1980	087	15:34:52	79.1	48087.0	-35.6	34.4	-2.9	-44.2
0733	0557	14 JUN 1980	166	06:54:00	60.3	49686.7	3.6	22.0	0.4	82.3
0734	0557	14 JUN 1980	166	16:[illegible]5:22	57.5	47274.7	-35.5	34.6	0.4	83.0
0735	0558	15 JUN 1980	167	02:20:35	58.3	65170.5	-10.0	25.9	0.4	83.6
0736	0558	15 JUN 1980	167	06:56:20	61.8	50033.1	3.4	22.1	0.5	83.9
0740	0559	16 JUN 1980	168	16:51:51	60.0	46684.7	-35.9	34.7	0.6	86.1
0742	0560	17 JUN 1980	169	02:54:27	61.7	64573.1	-9.1	25.6	0.6	86.8
0743	0560	17 JUN 1980	169	07:22:36	65.2	48755.8	4.3	21.9	0.6	87.1
0744	0587	14 JUL 1980	196	10:07:30	108.0	46590.2	5.8	21.6	2.7	130.0
0747	0589	16 JUL 1980	198	05:46:15	107.6	63807.5	-8.3	25.5	2.8	132.8
0748	0589	16 JUL 1980	198	10:07:42	111.0	47284.3	5.2	21.7	2.8	133.1
0749	0590	17 JUL 1980	199	10:18:35	112.7	46575.4	5.7	21.6	2.9	134.7
0750	0591	18 JUL 1980	200	06:01:23	110.8	63523.0	-8.0	25.4	2.9	136.0
0751	0591	18 JUL 1980	200	10:21:51	114.2	46560.6	5.8	21.6	2.9	136.3
0752	0592	19 JUL 1980	201	06:04:34	112.4	63527.0	-8.0	25.4	3.0	137.6
0753	0592	19 JUL 1980	201	10:26:34	115.8	46405.0	5.9	21.5	3.0	137.9
0754	0593	20 JUL 1980	202	06:06:33	114.0	63556.2	-8.0	25.4	3.0	139.2
0755	0593	20 JUL 1980	202	10:27:14	117.4	46602.4	5.7	21.6	3.0	139.5

ORIGINAL PAGE IS
OF POOR QUALITY

Table I (continued)

Map#	Orb#	Date	DOY	HH:MM:SS	Phase (Deg)	Range (Km)	C e l e s t i a l SCLAT	SCLON	SSLAT	SSLON
0757	0594	21 JUL 1980	203	10:31:17	118.9	46517.5	5.6	21.6	3.1	141.1
0759	0595	22 JUL 1980	204	10:19:49	120.3	47953.1	4.7	21.8	3.1	142.6
0760	0596	23 JUL 1980	205	06:00:46	118.5	64046.0	-8.7	25.6	3.1	143.9
0761	0596	23 JUL 1980	205	10:21:35	121.9	48044.9	4.7	21.9	3.1	144.2
0762	0597	24 JUL 1980	206	06:01:47	120.0	64107.9	-8.7	25.6	3.2	145.5
0763	0597	24 JUL 1980	206	10:23:[illegible]9	123.5	48103.3	4.6	21.9	3.2	145.8
0764	0598	25 JUL 1980	207	06:02:27	121.6	64158.2	-8.8	25.6	3.2	147.1
0765	0598	25 JUL 1980	207	10:24:50	125.0	48294.8	4.5	21.9	3.2	147.4
0768	0600	27 JUL 1980	209	06:11:42	124.7	64295.6	-9.0	25.7	3.3	150.3
0769	0600	27 JUL 1980	209	10:35:45	128.2	48542.7	4.3	21.9	3.3	150.6

Table II. Observations used in Figure 11.

Row	Column	Map #	Phase
1	1	110	1.1o
1	2	104	4.0
1	3	94	11.9
1	4	313	14.7
1	5	140	20.1
1	6	127	24.0
2	1	428	29.8
2	2	93	35.4
2	3	67	40.0
2	4	56	44.2
2	5	172	48.8
2	6	83	53.4
3	1	500	59.1
3	2	509	65.3
3	3	36	70.9
3	4	524	74.8
3	5	191	80.4
3	6	542	86.4
4	1	708	89.6
4	2	196	94.5
4	3	199	99.1
4	4	21	105.8
4	5	10	109.9
4	6	577	115.7
5	1	578	119.3
5	2	683	125.4
5	3	218	129.5
5	4	617	135.9
5	5	223	140.8
5	6	219	145.2

Table III. Latitudinally averaged results on the movements of polarization features. Bin width is 15o of latitude.

Wavelength	Latitude	Number	Avg. Zonal speed	RMS Deviation
270 nm	59.0o	1	-27.8 ms^{-1}	-
	43.0	1	-98.9	-
	21.7	3	-129.3	79.5
	6.0	1	-80.7	-
	-5.5	4	-92.4	20.1
	-18.3	3	-86.4	0.2
	-35.0	3	-128.3	14.3
	-53.5	2	-76.8	16.6
365 nm	34.3	6	-42.2	14.9
	24.0	5	-74.4	13.9
	7.4	11	-79.4	22.4
	-4.5	19	-62.4	25.2
	-19.8	11	-73.5	24.0
	-35.1	11	-67.9	19.5
	-60.3	3	-45.1	0.6
550 nm	48.3	2	-34.4	-
	35.5	4	-50.9	11.3
	18.5	7	-63.2	20.1
	5.6	13	-68.6	27.1
	-6.4	22	-79.7	23.3
	-19.9	11	-56.8	15.3
	-36.8	4	-93.7	42.2
	-47.3	2	-63.7	-
935 nm	-8.0	3	-66.3	27.4
	-22.7	3	-66.7	31.7
	-38.5	4	-70.1	24.3

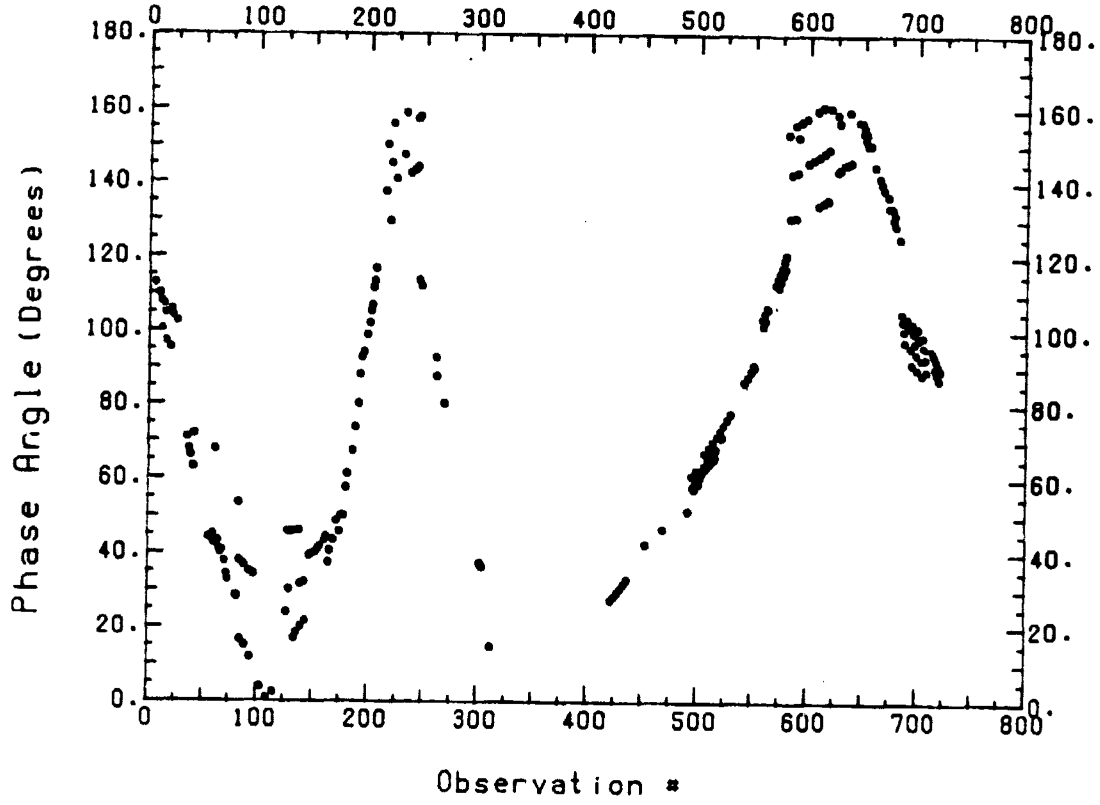
Phase Angle (Degrees)
Observation #
0
100
200
300
400
500
600
700
800
0.
20.
40.
60.
80.
100.
120.
140.
160.
180.

Figure 1

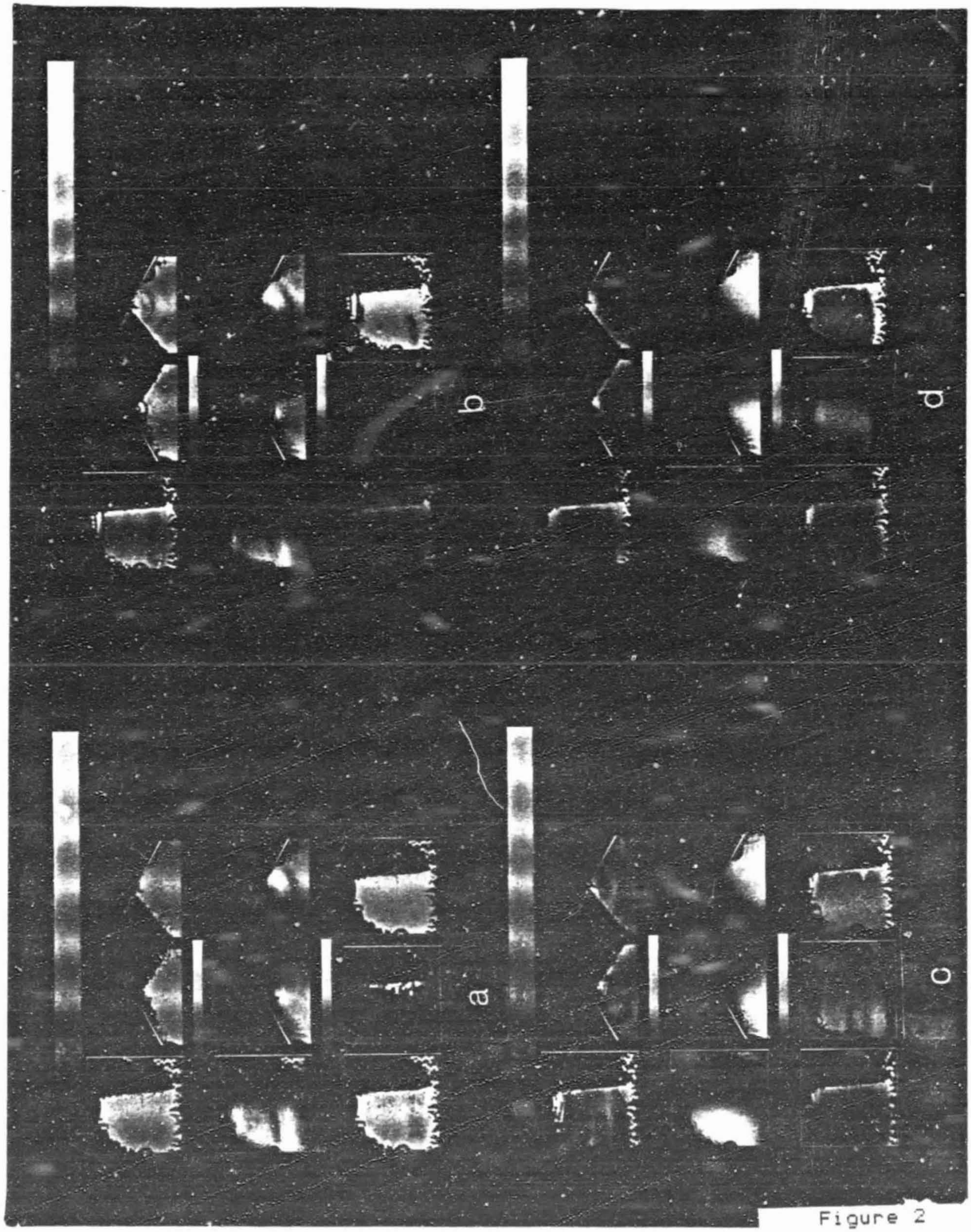

Figure 2

704	1	88.50	A0=	200.70	A1=	0.91967	RSQ=	0.87131	N=	1020	ZEN<	85.00
704	2	88.50	A0=	8367.49	A1=	0.89857	RSQ=	0.86337	N=	1017	ZEN<	85.00
704	3	88.50	A0=	4650.02	A1=	1.13206	RSQ=	0.97280	N=	1016	ZEN<	85.00
704	4	88.50	A0=	3460.36	A1=	1.12047	RSQ=	C.96792	N=	986	ZEN<	85.00

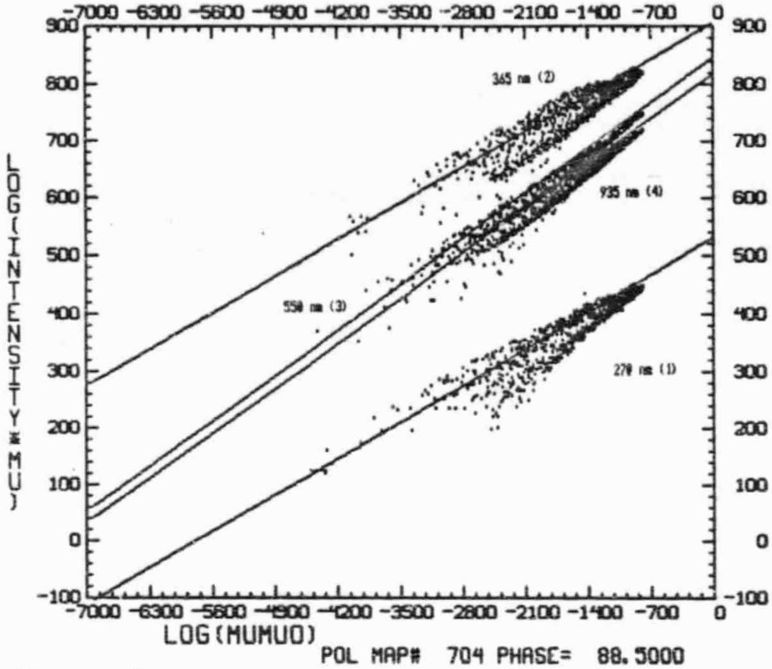

Figure 3a

705	1	99.00	A0=	261.36	A1=	0.98733	RSQ=	0.89960	N=	914	ZEN<	85.00
705	2	99.00	A0=	1.12+04	A1=	0.97480	RSQ=	0.88362	N=	936	ZEN<	85.00
705	3	99.00	A0=	4960.11	A1=	1.11886	RSQ=	0.96045	N=	926	ZEN<	85.00
705	4	99.00	A0=	3806.11	A1=	1.11715	RSQ=	0.95301	N=	937	ZEN<	85.00

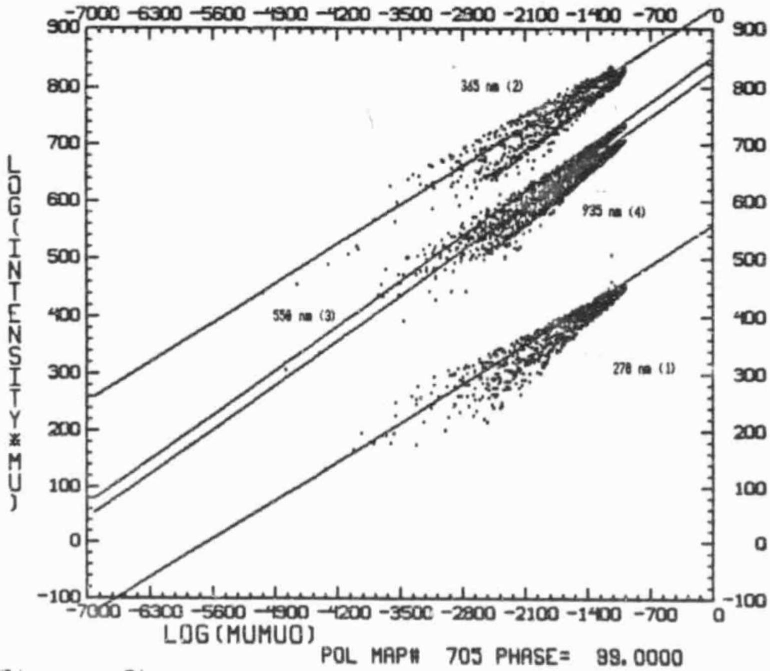

Figure 3b

104	1	4.00	A0=	370.47	A1=	0.64479	RSQ=	0.92300	N=	2131	ZEN< 85.00
104	2	4.00	A0=	9244.21	A1=	0.75591	RSQ=	0.93331	N=	2096	ZEN< 85.00
104	3	4.00	A0=	4855.17	A1=	1.06486	RSQ=	0.99450	N=	2098	ZEN< 85.00
104	4	4.00	A0=	3550.47	A1=	1.05433	RSQ=	0.99483	N=	2103	ZEN< 85.00

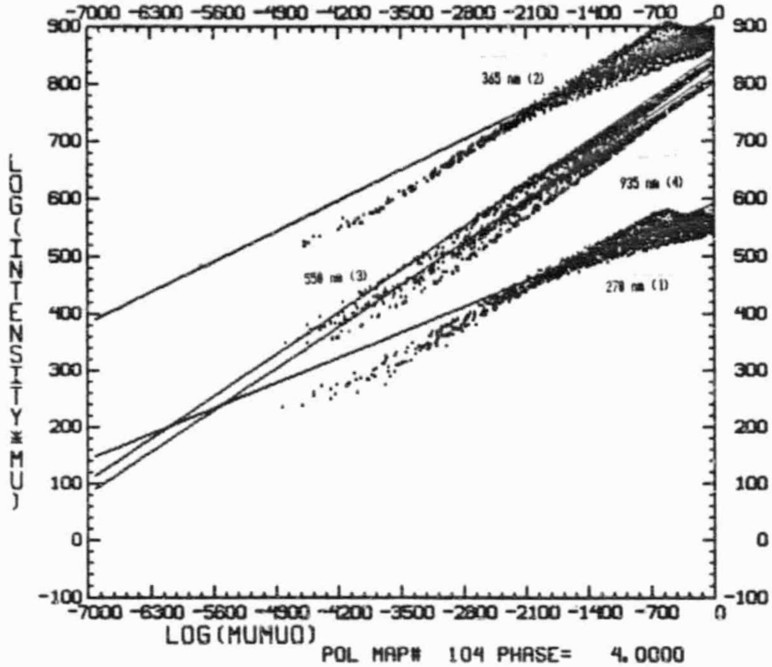

Figure 3c

94	1	11.89	A0=	353.97	A1=	0.65066	RSQ=	0.94715	N=	2062	ZEN< 85.00
94	2	11.89	A0=	9222.31	A1=	0.78675	RSQ=	0.96724	N=	2098	ZEN< 85.00
94	3	11.89	A0=	4917.14	A1=	1.08067	RSQ=	0.99554	N=	2073	ZEN< 85.00
94	4	11.89	A0=	3570.46	A1=	1.06330	RSQ=	0.99450	N=	2074	ZEN< 85.00

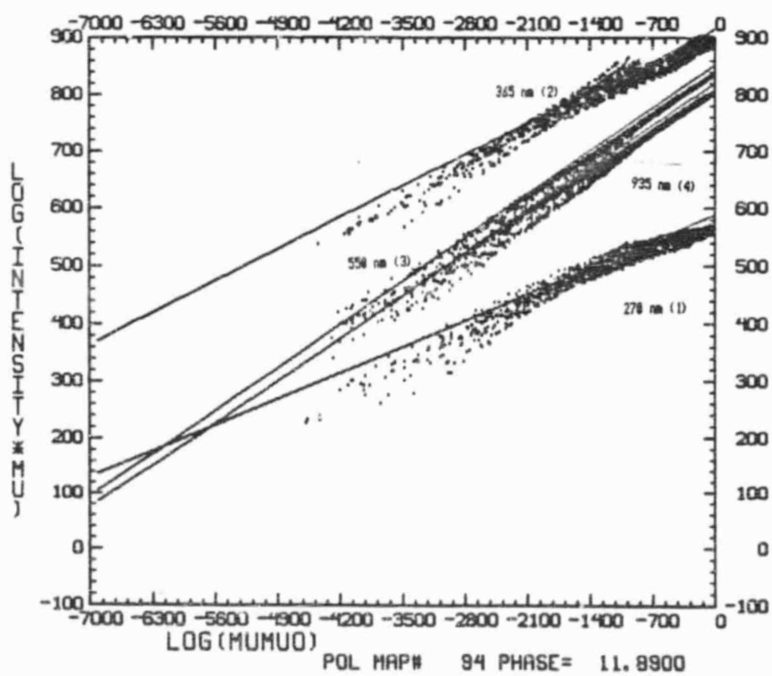

Figure 3d

ORIGINAL PAGE IS
OF POOR QUALITY

82	1	28.60	A0=	276.49	A1=	0.66504	RSQ=	0.90995	N=	2062	ZEN<	85.00
82	2	28.60	A0=	7476.30	A1=	0.79521	RSQ=	0.93213	N=	2067	ZEN<	85.00
82	3	28.60	A0=	4441.55	A1=	1.11697	RSQ=	0.99637	N=	2037	ZEN<	85.00
82	4	28.60	A0=	3299.21	A1=	1.07721	RSQ=	0.99577	N=	2068	ZEN<	85.00

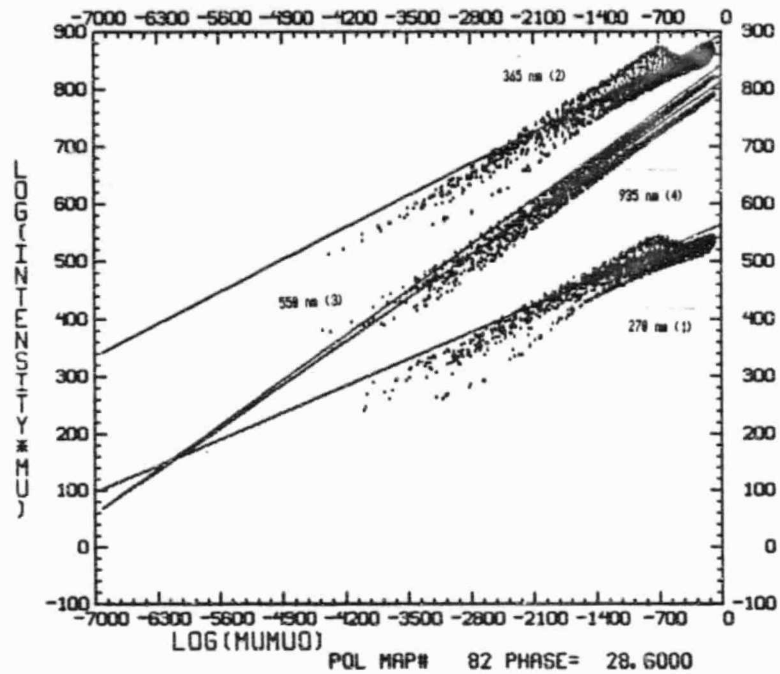

Figure 3e

453	1	42.80	A0=	136.20	A1=	0.63416	RSQ=	0.76529	N=	2058	ZEN<	85.00
453	2	42.80	A0=	6410.78	A1=	0.83486	RSQ=	0.89078	N=	2029	ZEN<	85.00
453	3	42.80	A0=	4102.31	A1=	1.13360	RSQ=	0.98822	N=	2032	ZEN<	85.00
453	4	42.80	A0=	3001.53	A1=	1.08840	RSQ=	0.98915	N=	1990	ZEN<	85.00

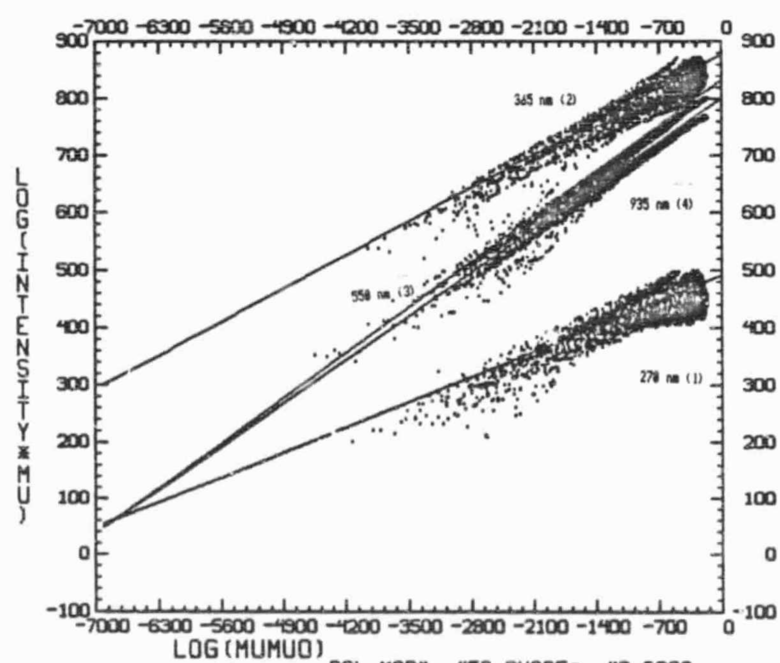

Figure 3f

492	1	51.80	A0=	146.00	A1=	0.74785	RSQ=	0.83633	N=	1743	ZEN<	85.00
492	2	51.80	A0=	6492.21	A1=	0.89993	RSQ=	0.85973	N=	1758	ZEN<	85.00
492	3	51.80	A0=	4179.44	A1=	1.18263	RSQ=	0.99428	N=	1746	ZEN<	85.00
492	4	51.80	A0=	3172.99	A1=	1.16281	RSQ=	0.99448	N=	1744	ZEN<	85.00

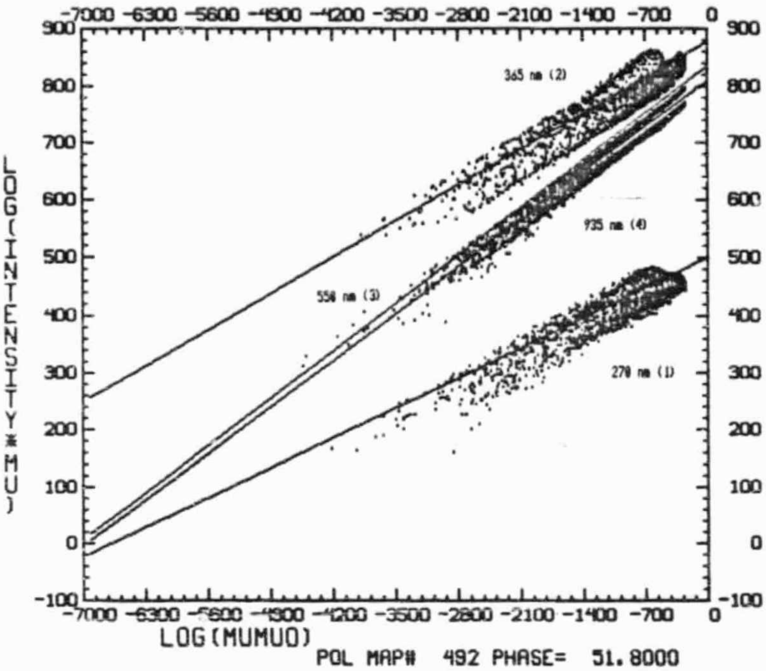

Figure 3g

499	1	62.69	A0=	139.55	A1=	0.72432	RSQ=	0.77075	N=	1496	ZEN<	85.00
499	2	62.69	A0=	6188.06	A1=	0.85562	RSQ=	0.82656	N=	1494	ZEN<	85.00
499	3	62.69	A0=	4194.04	A1=	1.16491	RSQ=	0.99212	N=	1467	ZEN<	85.00
499	4	62.69	A0=	3114.53	A1=	1.14236	RSQ=	0.99020	N=	1430	ZEN<	85.00

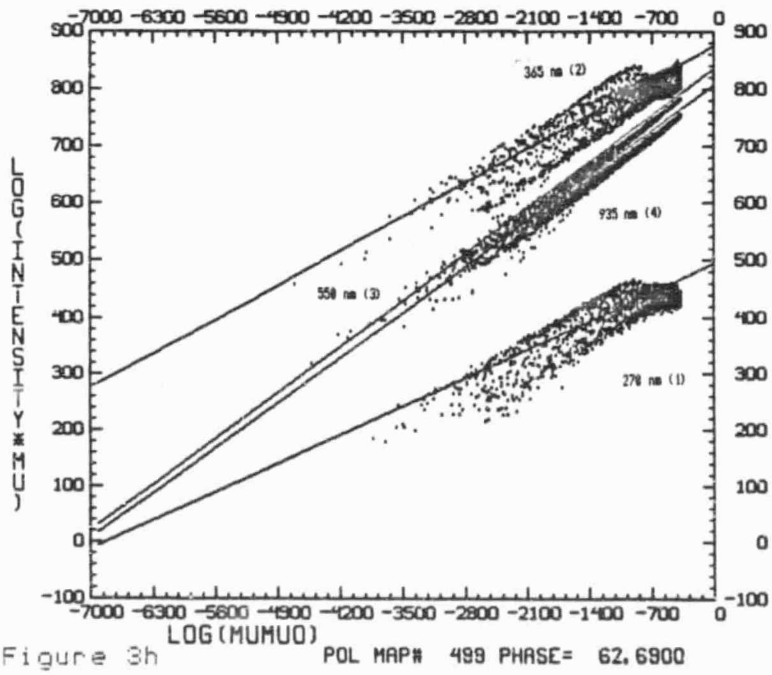

Figure 3h

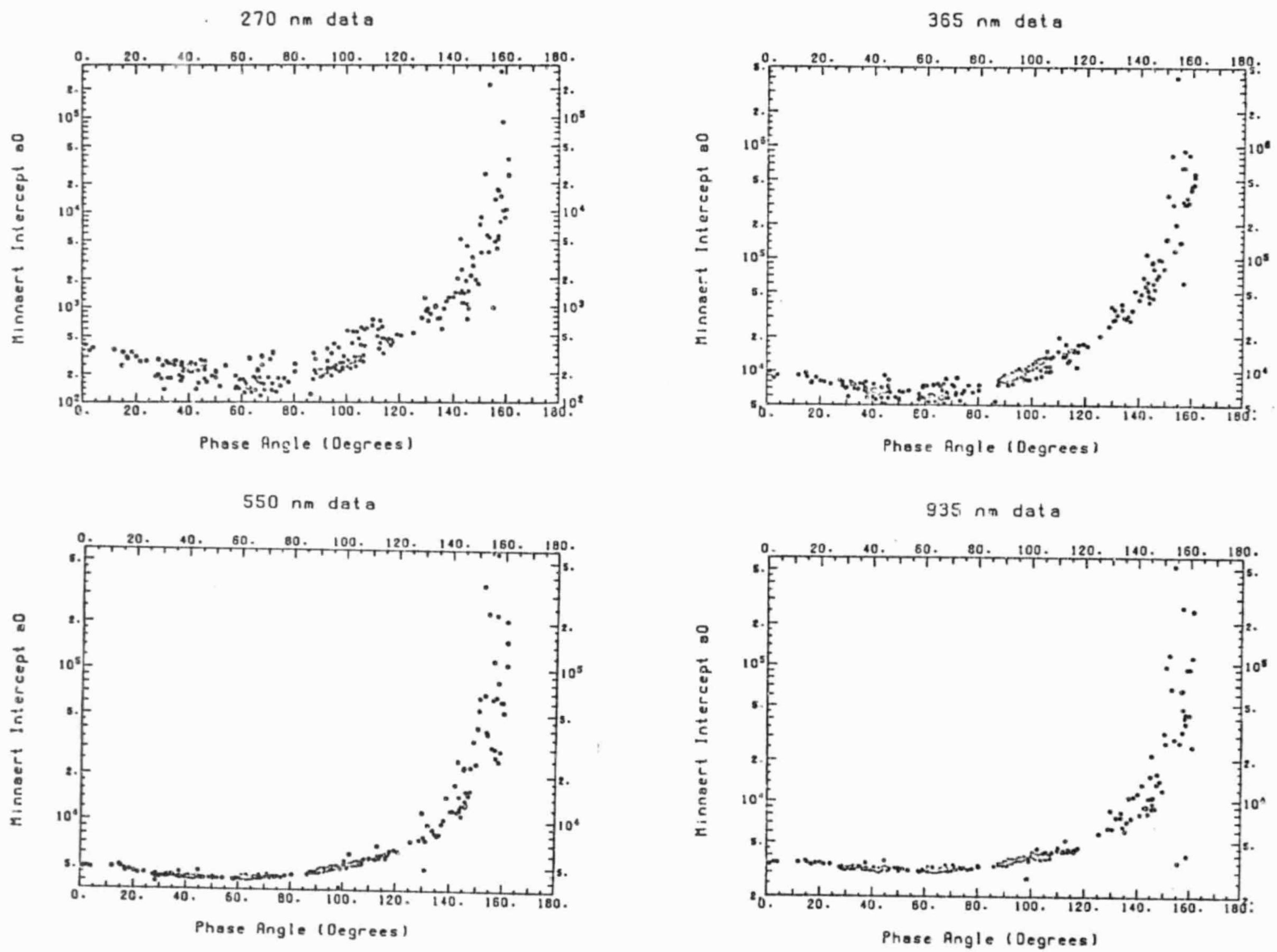
270 nm data
365 nm data
550 nm data
935 nm data
Minnaert Intercept a0
Phase Angle (Degrees)

Figure 4

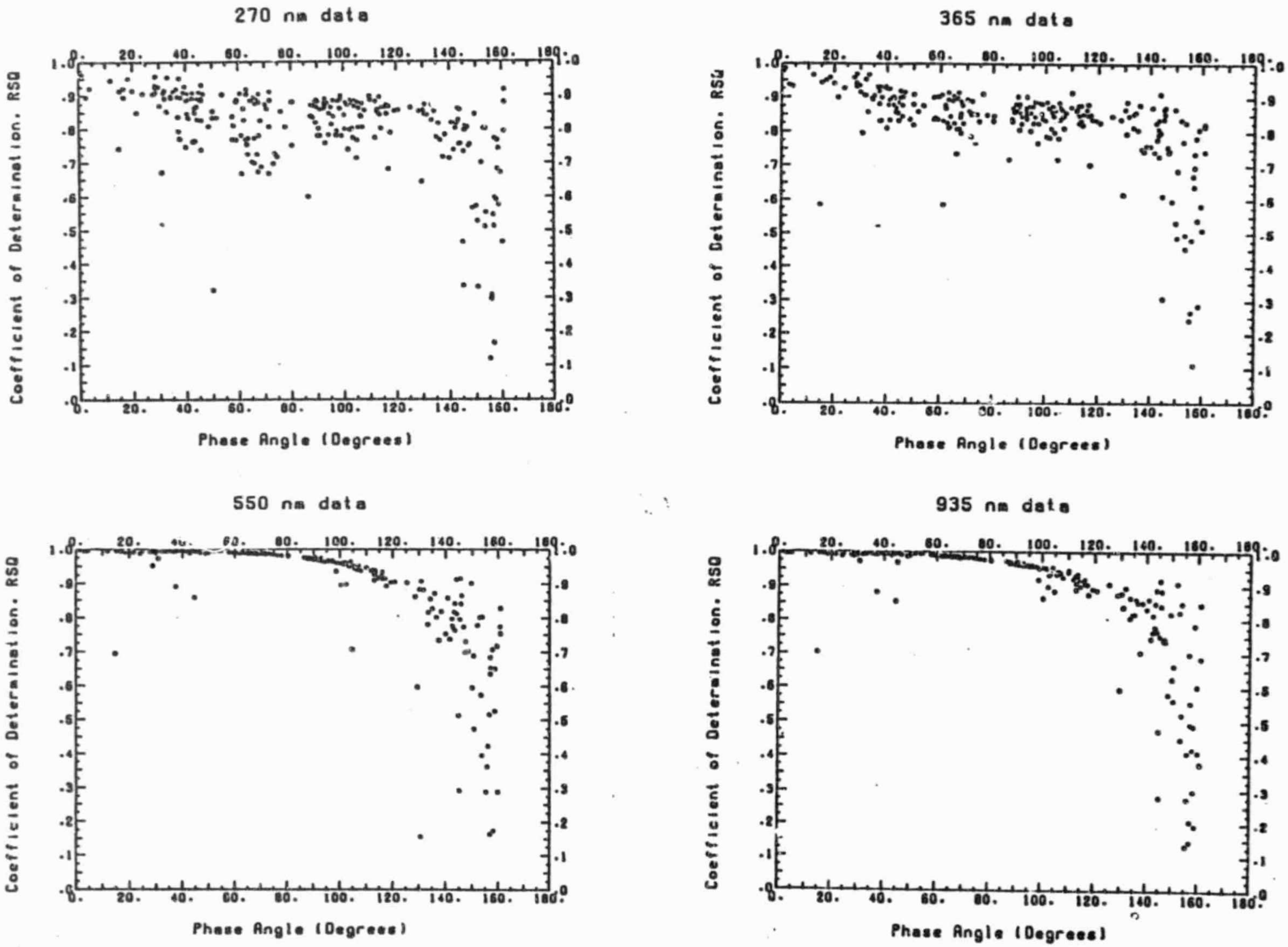
270 nm data
365 nm data
550 nm data
935 nm data
Coefficient of Determination. RSQ
Phase Angle (Degrees)

Figure 5

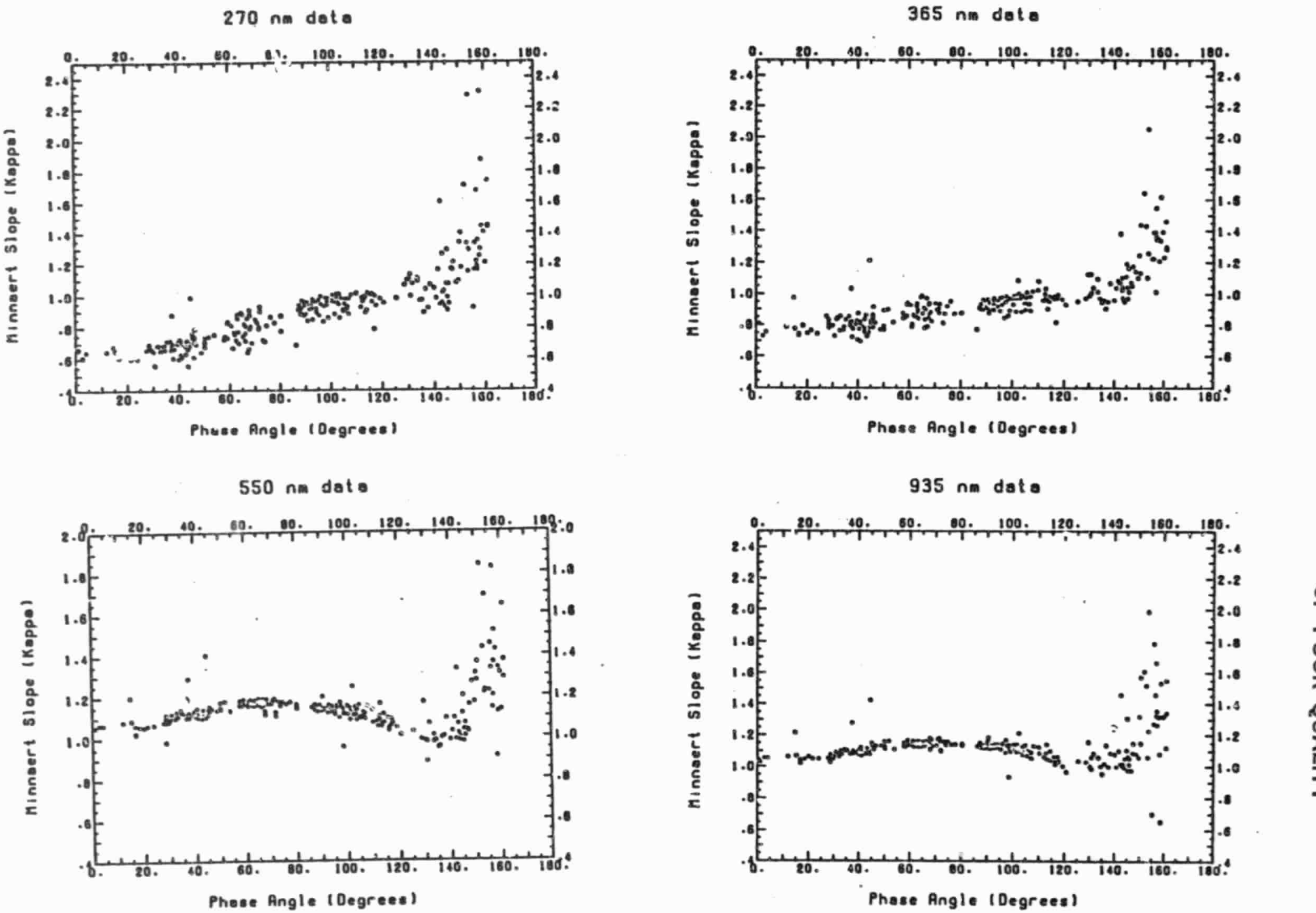
270 nm data
365 nm data
550 nm data
935 nm data
Minnaert Slope (Kappa)
Phase Angle (Degrees)

Figure 6

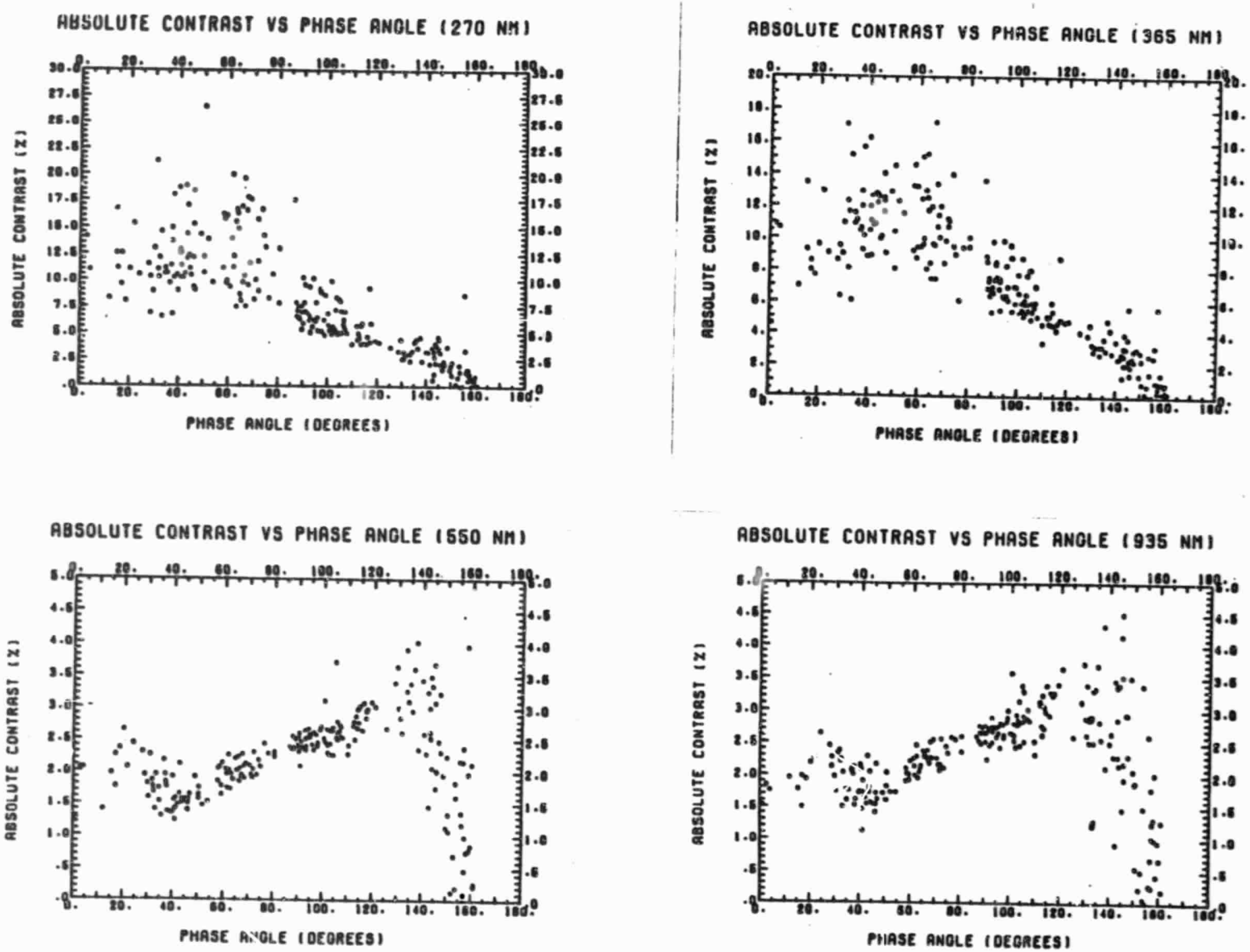
ABSOLUTE CONTRAST VS PHASE ANGLE (270 NM)
ABSOLUTE CONTRAST VS PHASE ANGLE (365 NM)
ABSOLUTE CONTRAST VS PHASE ANGLE (550 NM)
ABSOLUTE CONTRAST VS PHASE ANGLE (935 NM)
ABSOLUTE CONTRAST (%)
PHASE ANGLE (DEGREES)

Figure 7a

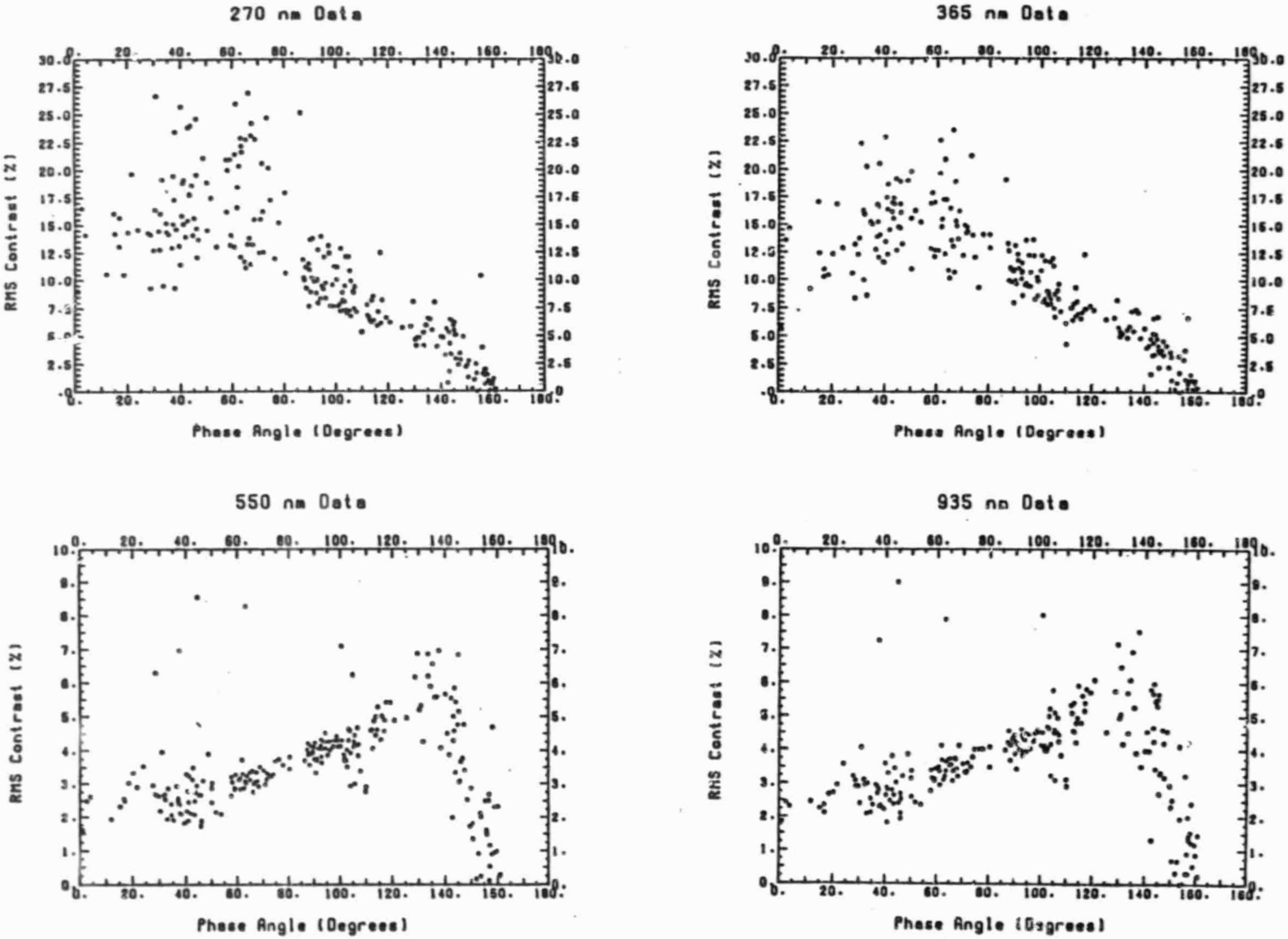
270 nm Data
RMS Contrast (%)
Phase Angle (Degrees)
365 nm Data
RMS Contrast (%)
Phase Angle (Degrees)
550 nm Data
RMS Contrast (%)
Phase Angle (Degrees)
935 nm Data
RMS Contrast (%)
Phase Angle (Degrees)

Figure 7b

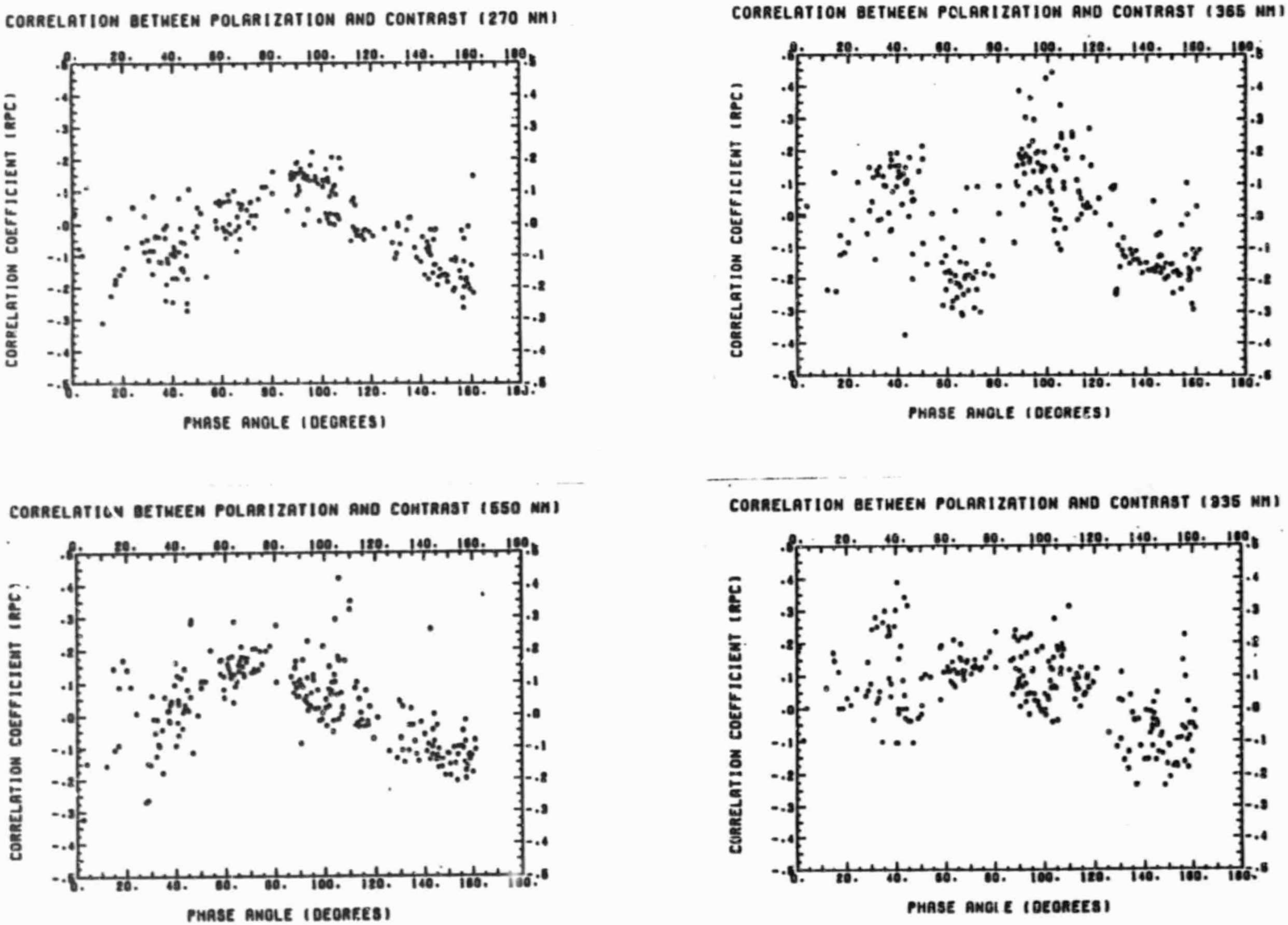

ORIGINAL PAGE IS
OF POOR QUALITY

Figure 8a

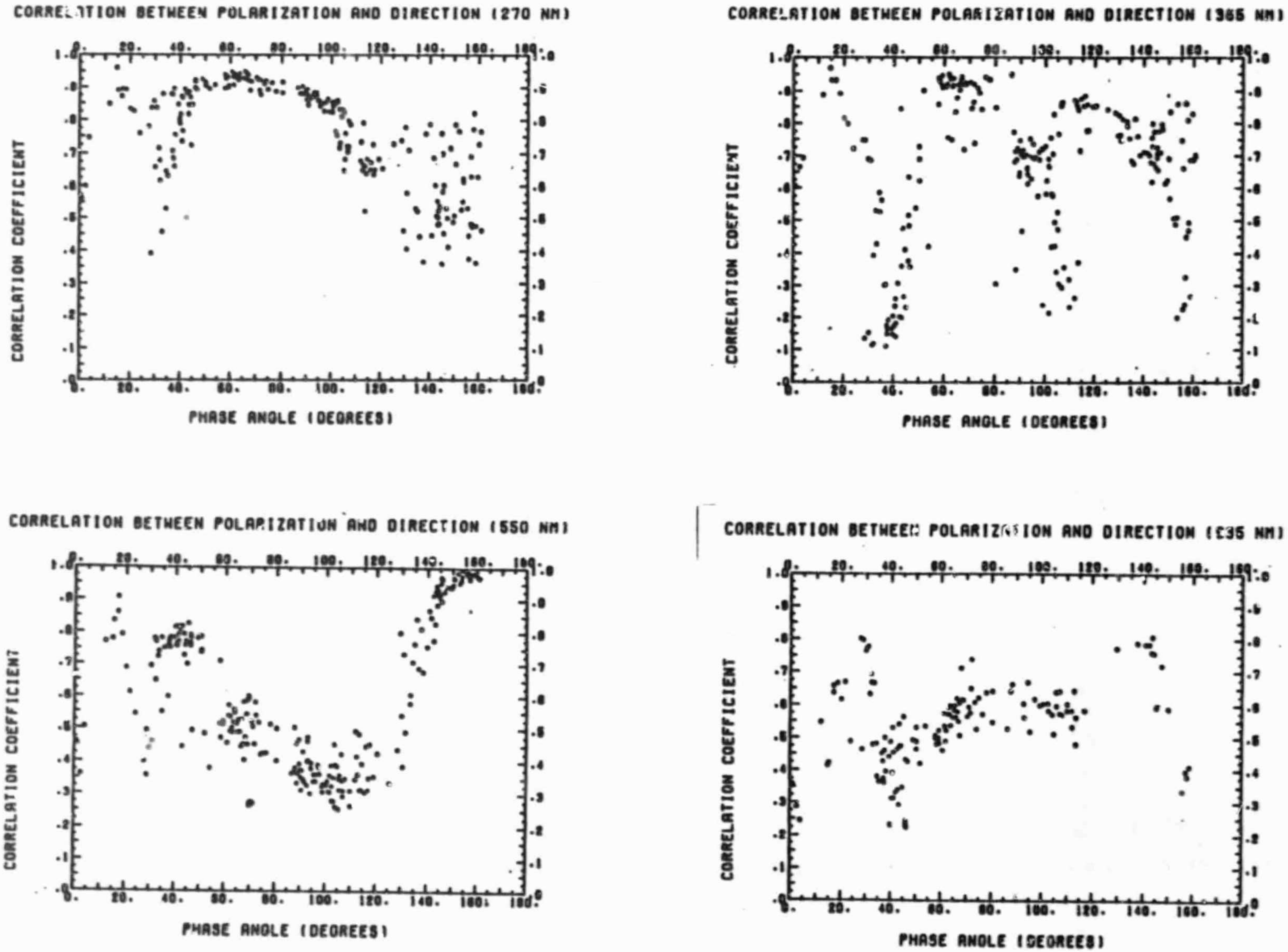
CORRELATION BETWEEN POLARIZATION AND DIRECTION (270 NM)
CORRELATION BETWEEN POLARIZATION AND DIRECTION (365 NM)
CORRELATION BETWEEN POLARIZATION AND DIRECTION (550 NM)
CORRELATION BETWEEN POLARIZATION AND DIRECTION (935 NM)
CORRELATION COEFFICIENT
PHASE ANGLE (DEGREES)

Figure 8b

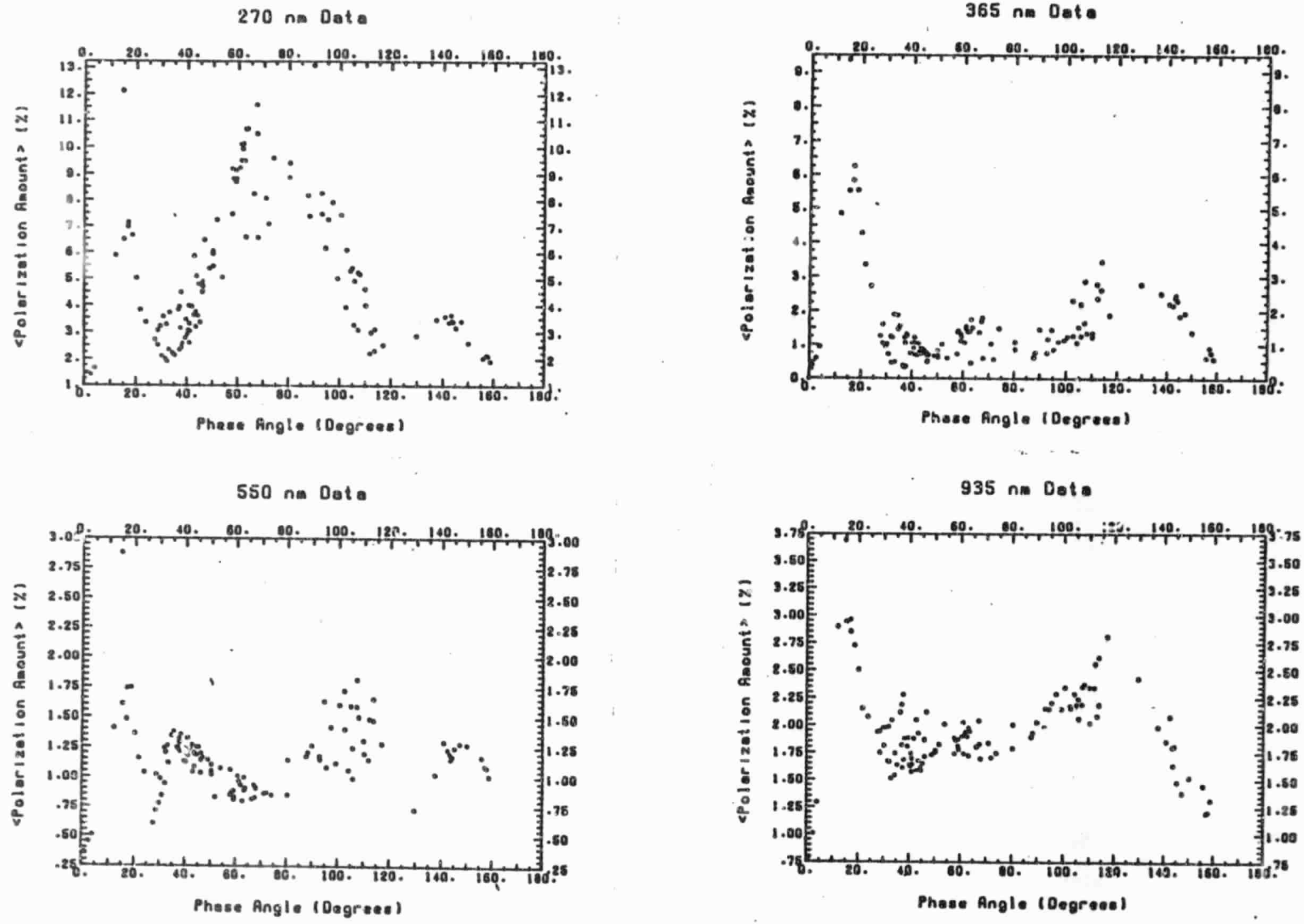
270 nm Data
365 nm Data
550 nm Data
935 nm Data
<Polarization Amount> (%)
Phase Angle (Degrees)

Figure 9a

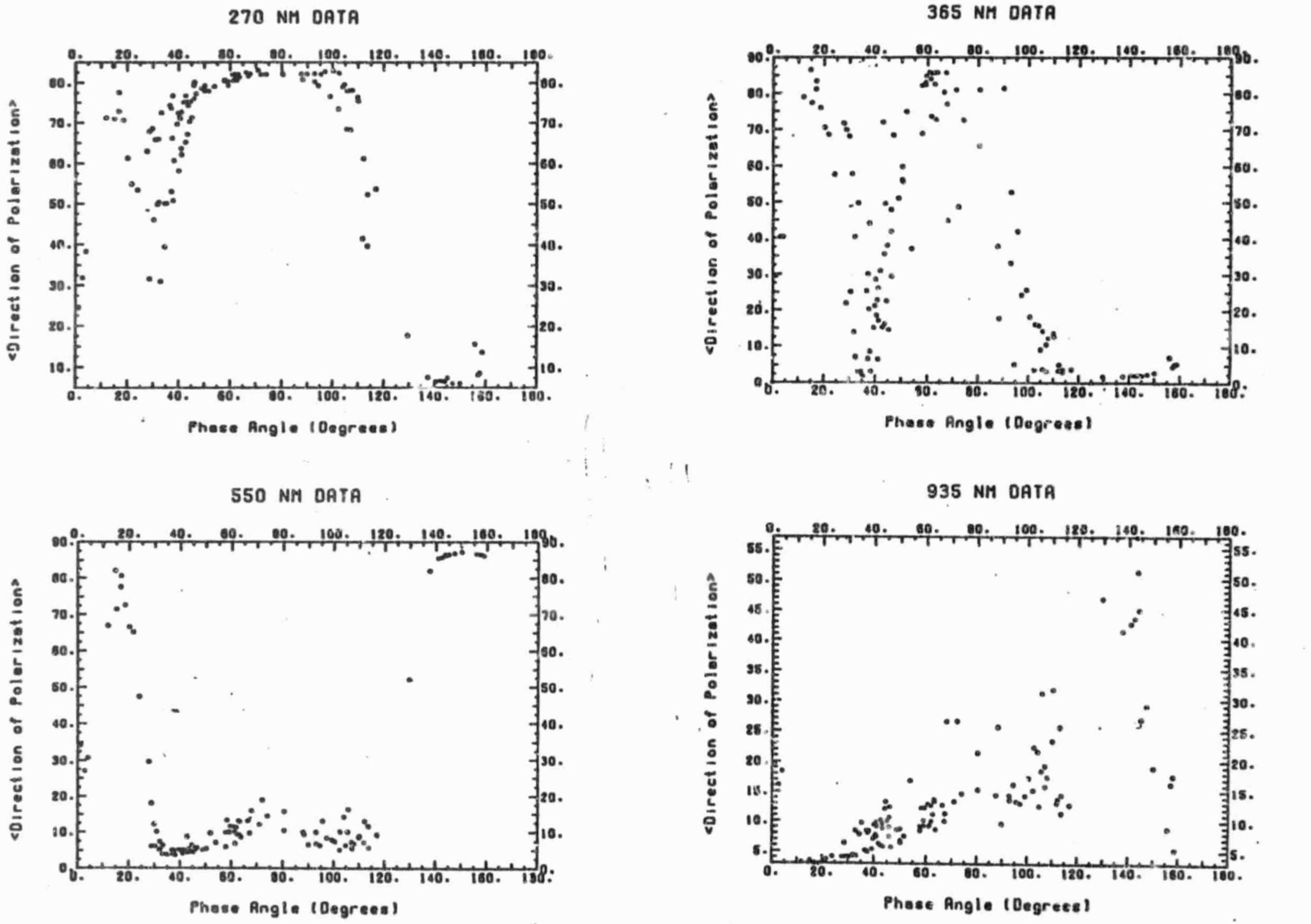
270 NM DATA
365 NM DATA
550 NM DATA
935 NM DATA
<Direction of Polarization>
Phase Angle (Degrees)

Figure 9b

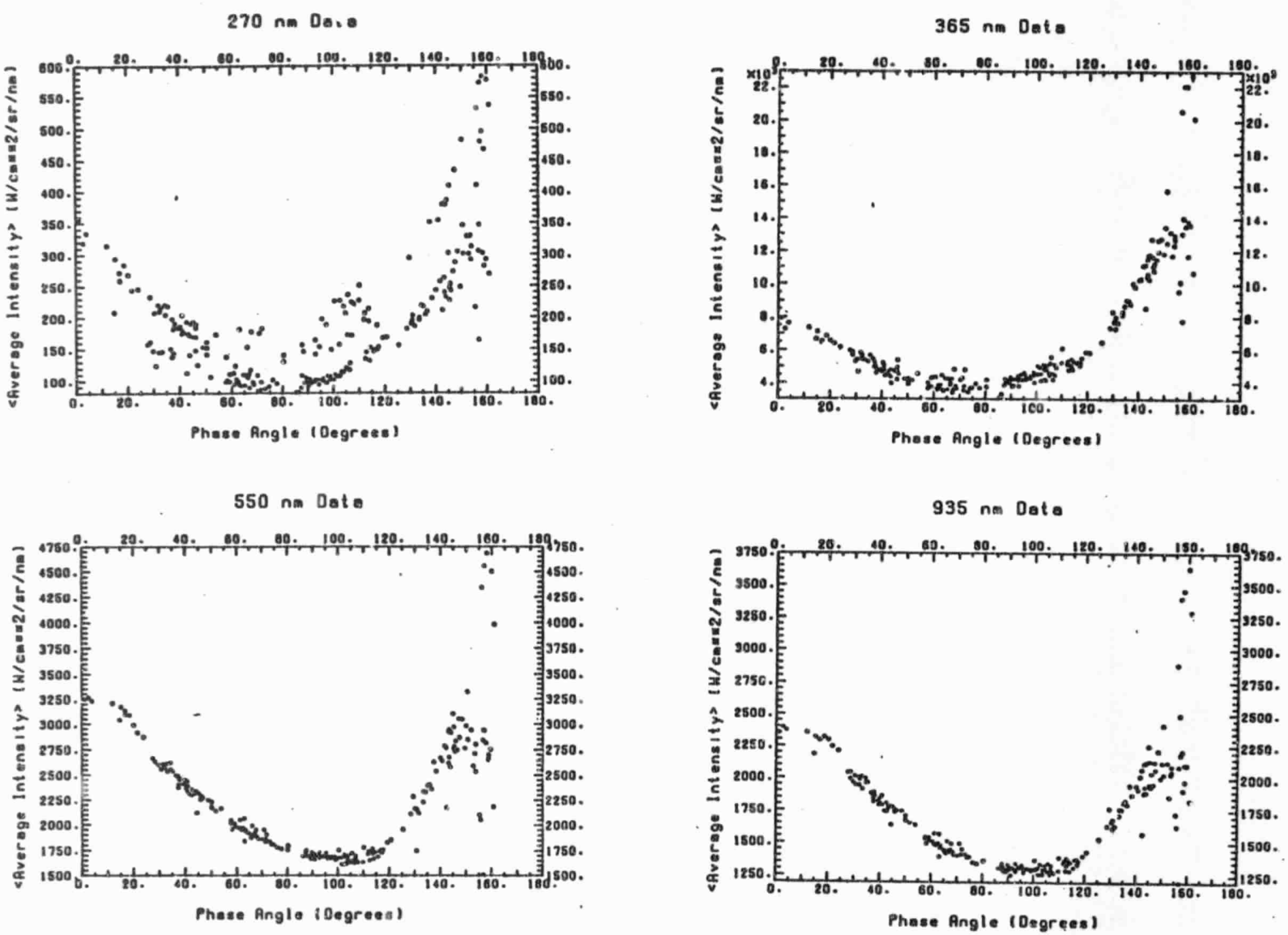
270 nm Data
365 nm Data
550 nm Data
935 nm Data
<Average Intensity> (W/cm**2/sr/nm)
Phase Angle (Degrees)

Figure 9c

ORIGINAL PAGE IS
OF POOR QUALITY

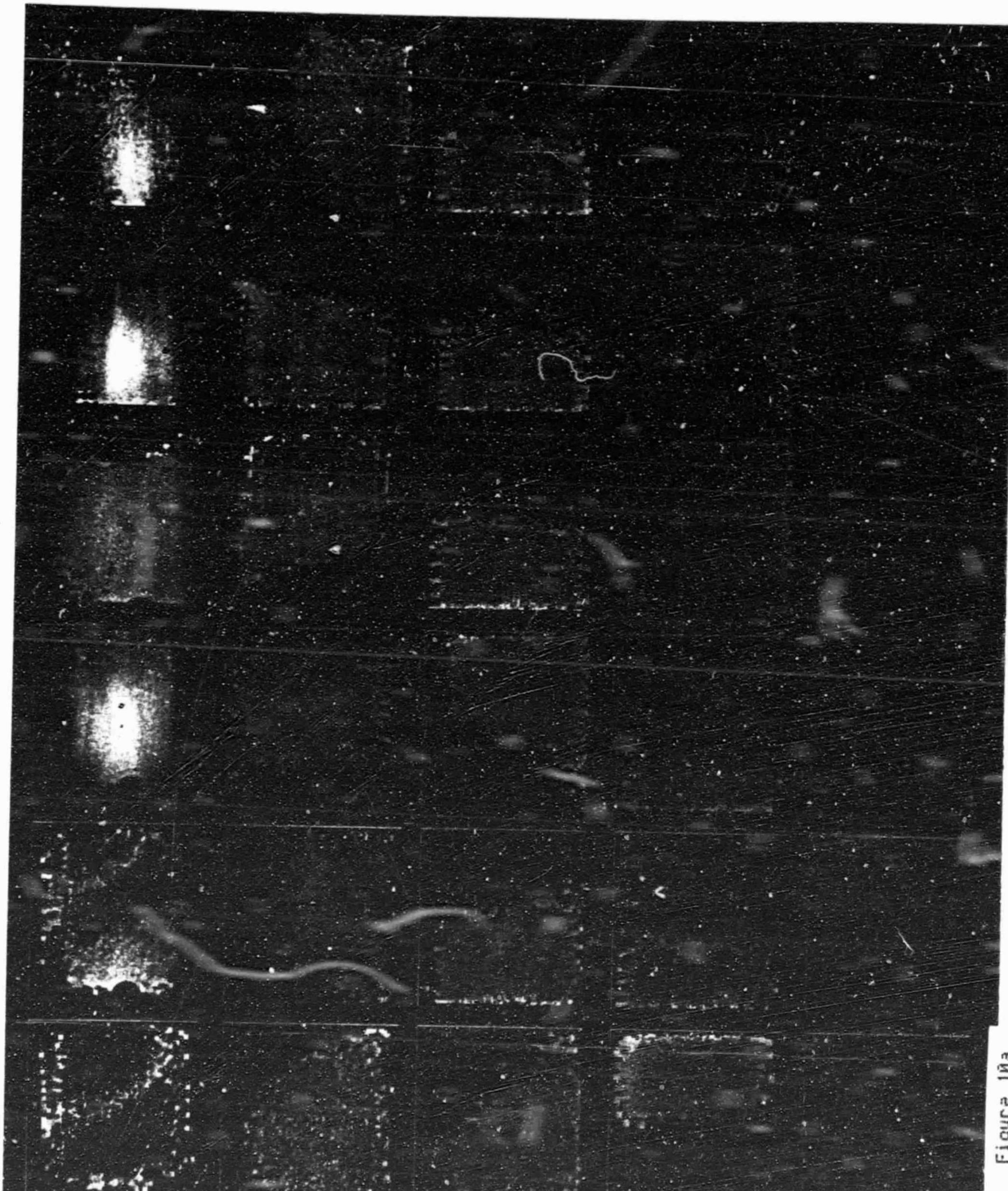

Figure 10a

Figure 10b

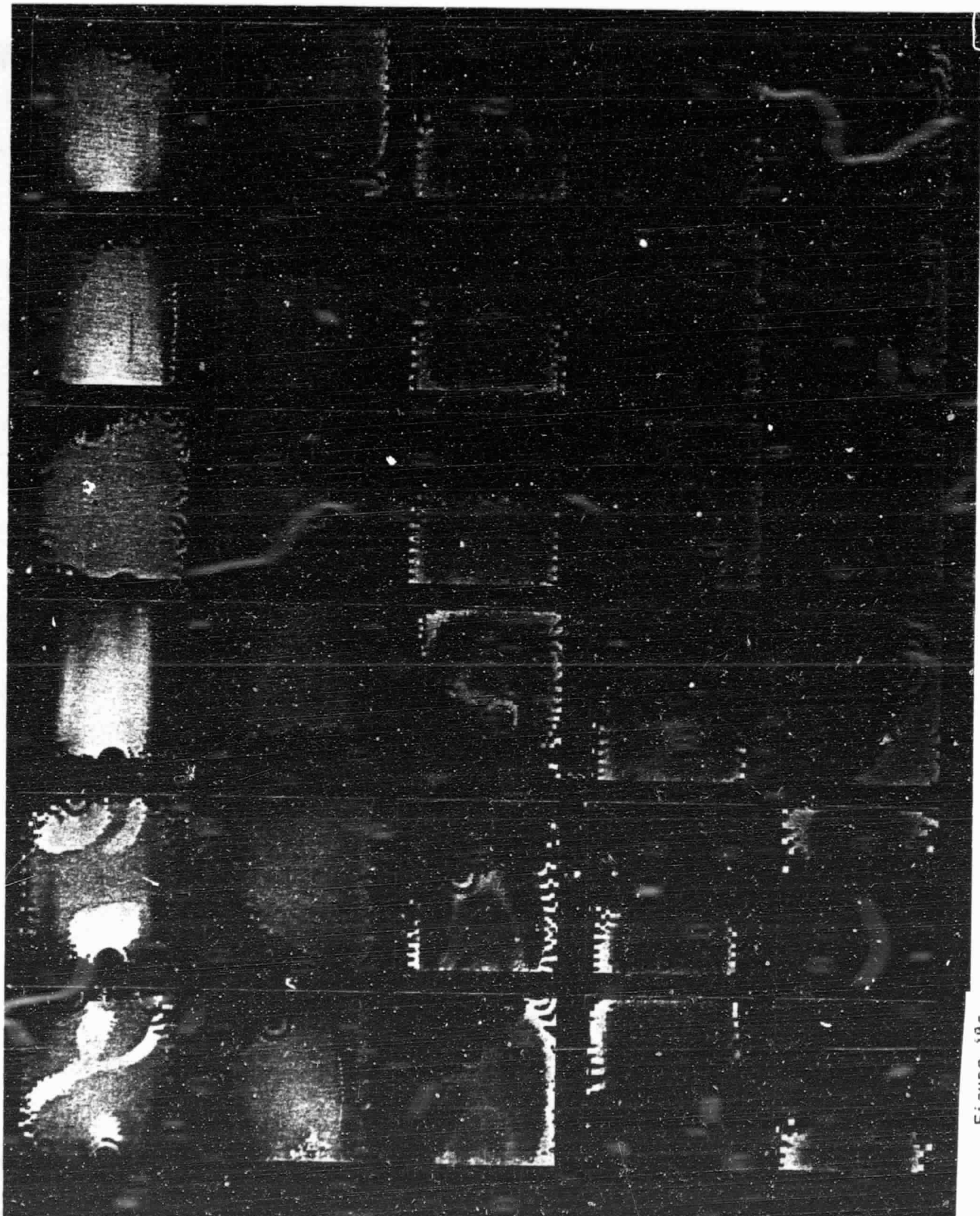

Figure 10c

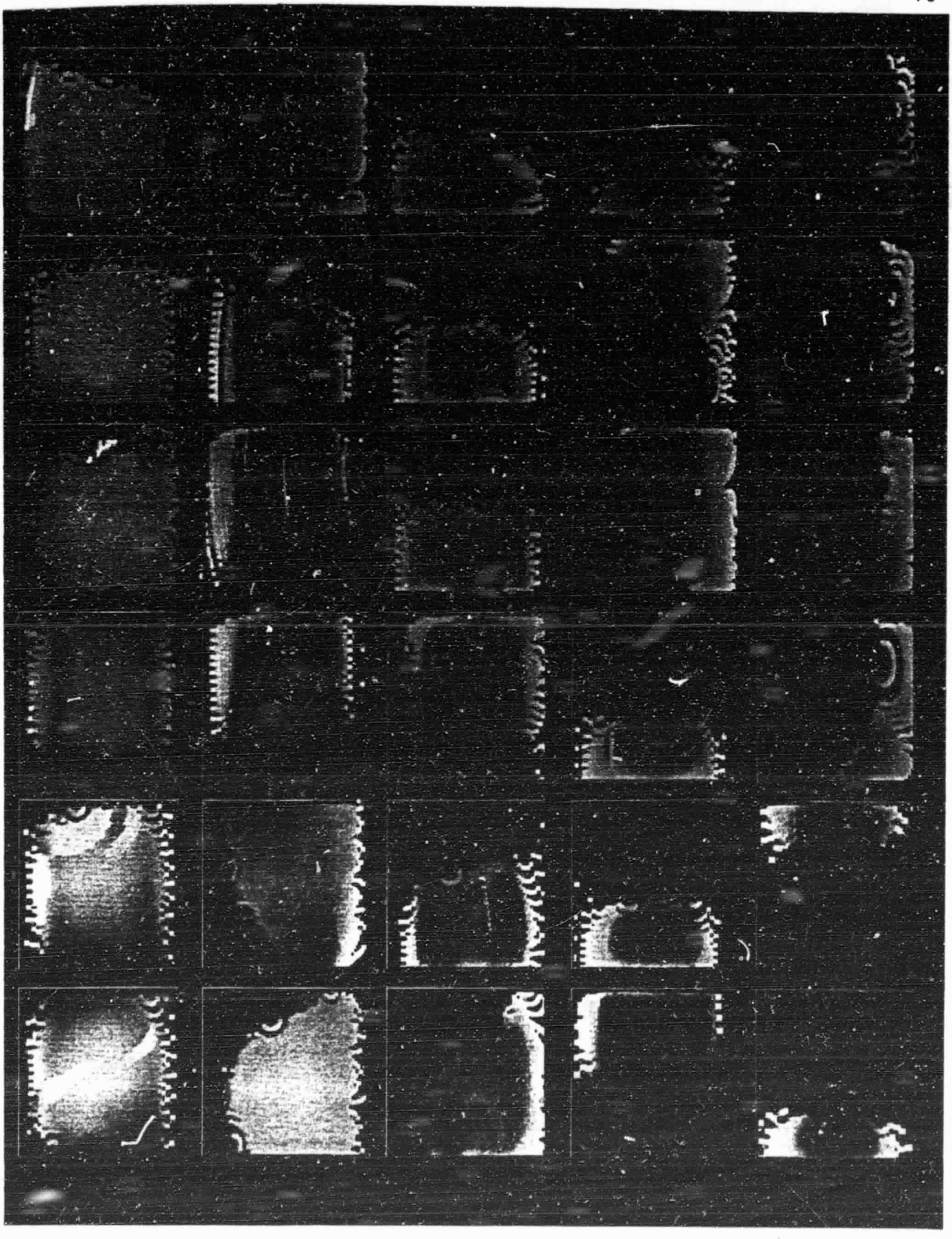

Figure 10d

ORIGINAL PAGE IS
OF POOR QUALITY

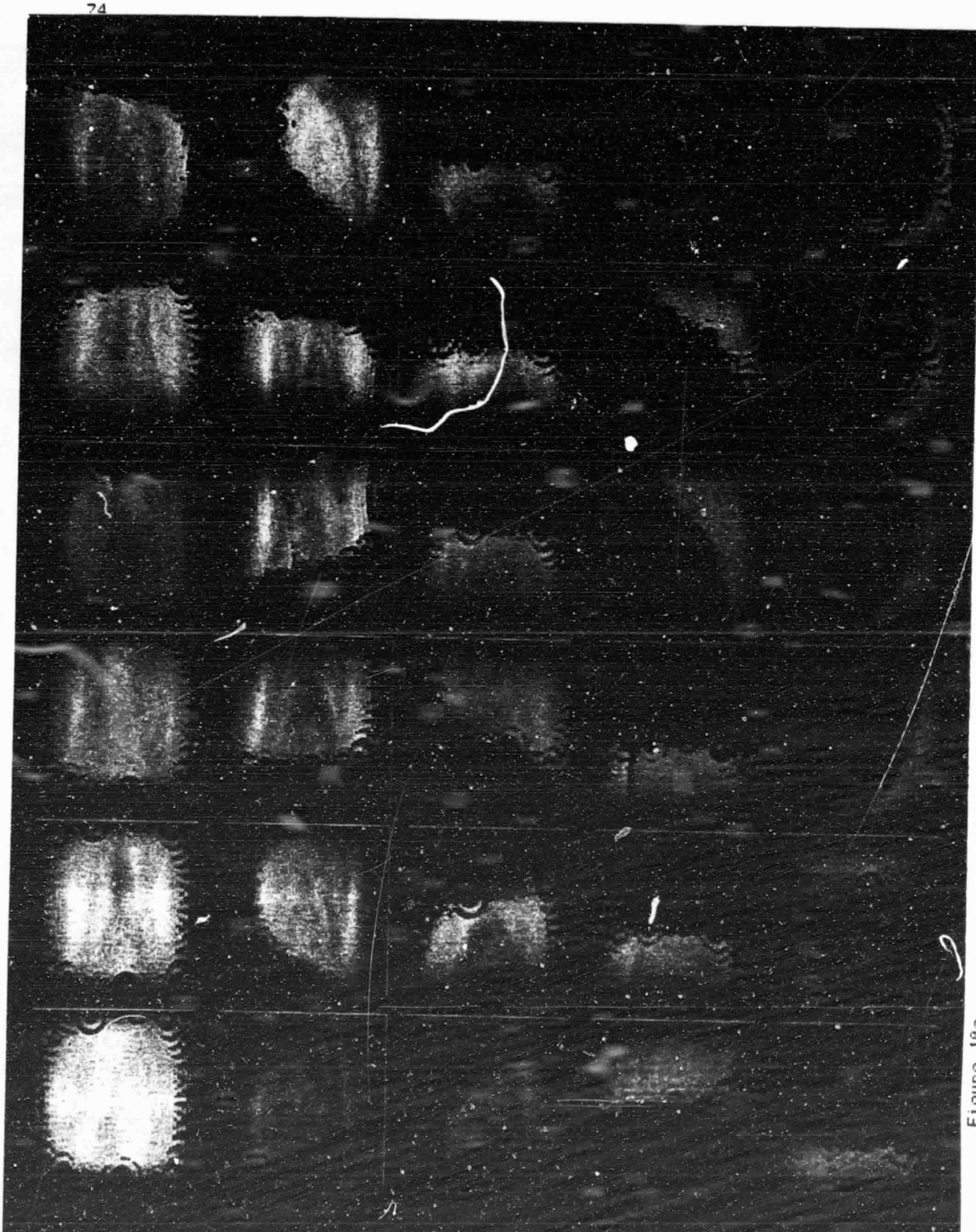

Figure 10e

Figure 10f

Figure 11

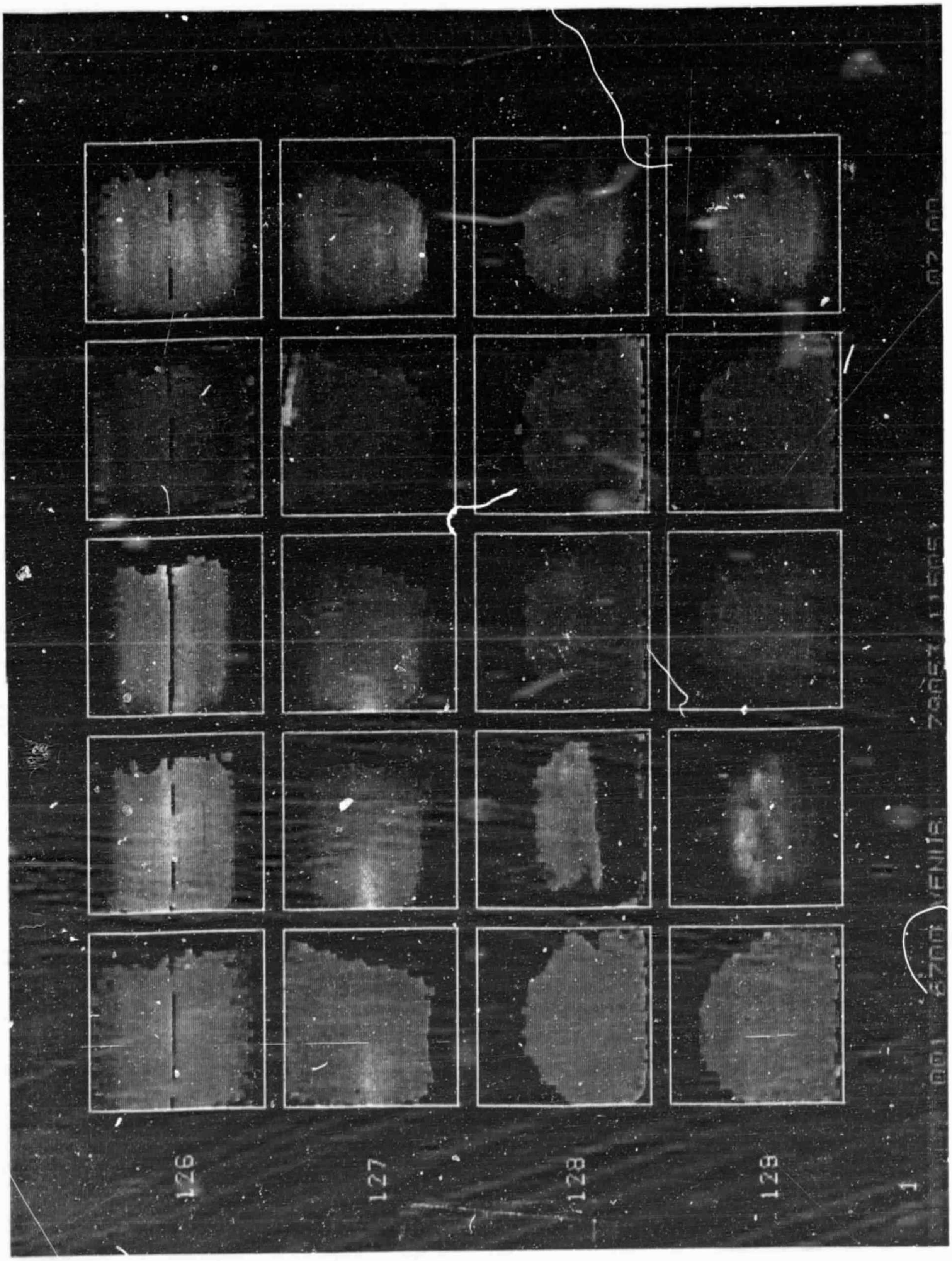

Figure 12a

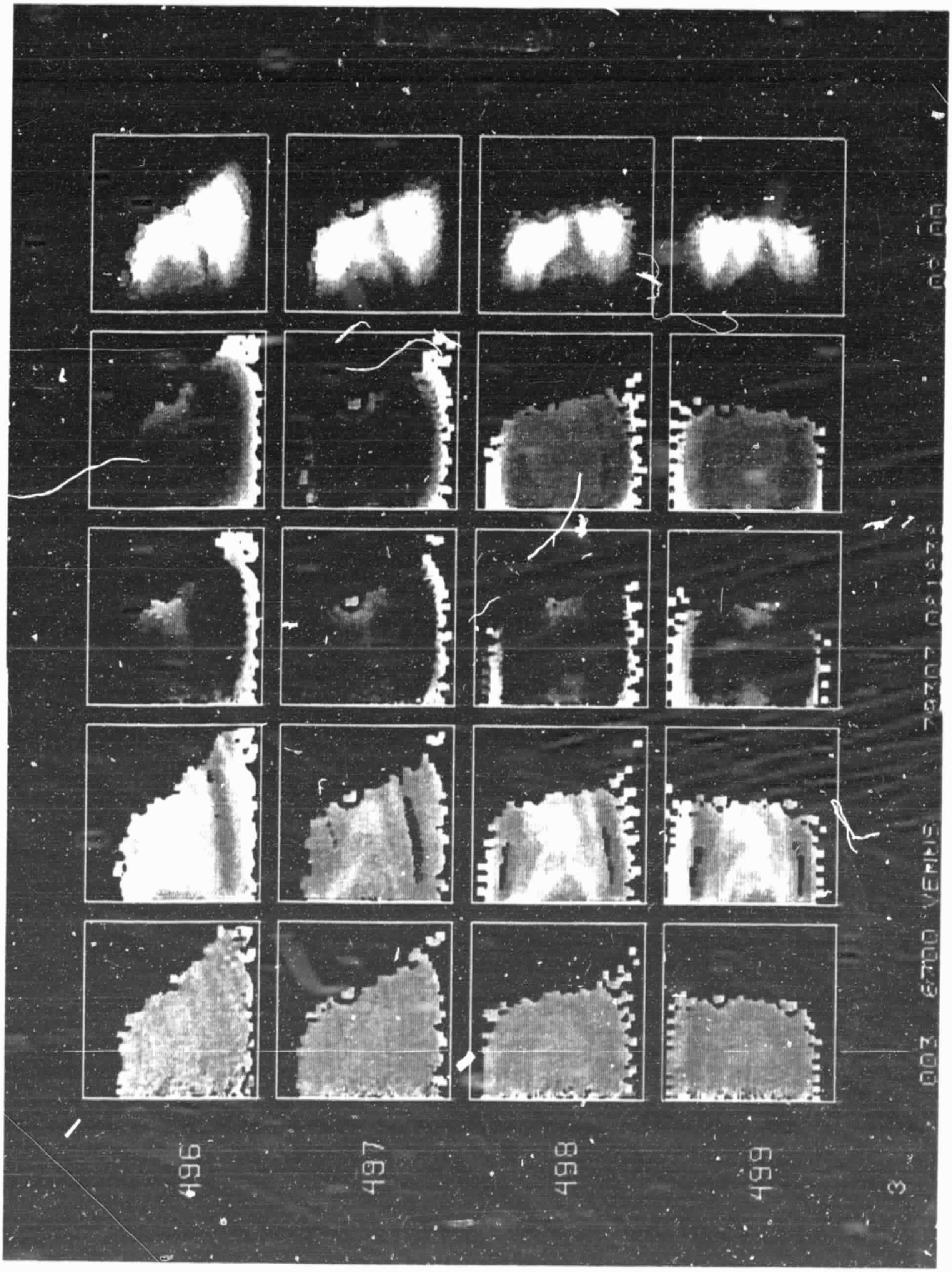

Figure 12b

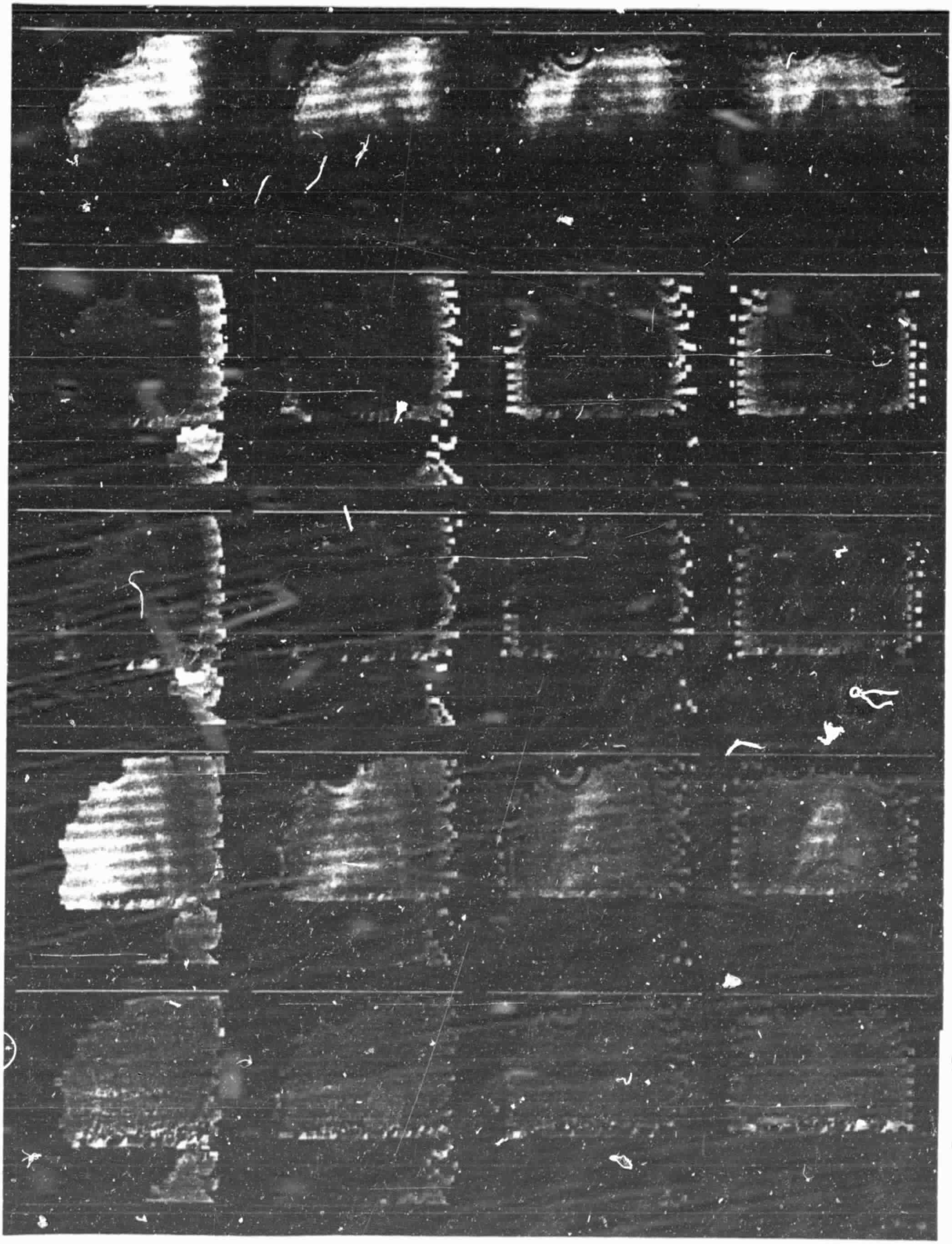

Figure 12c

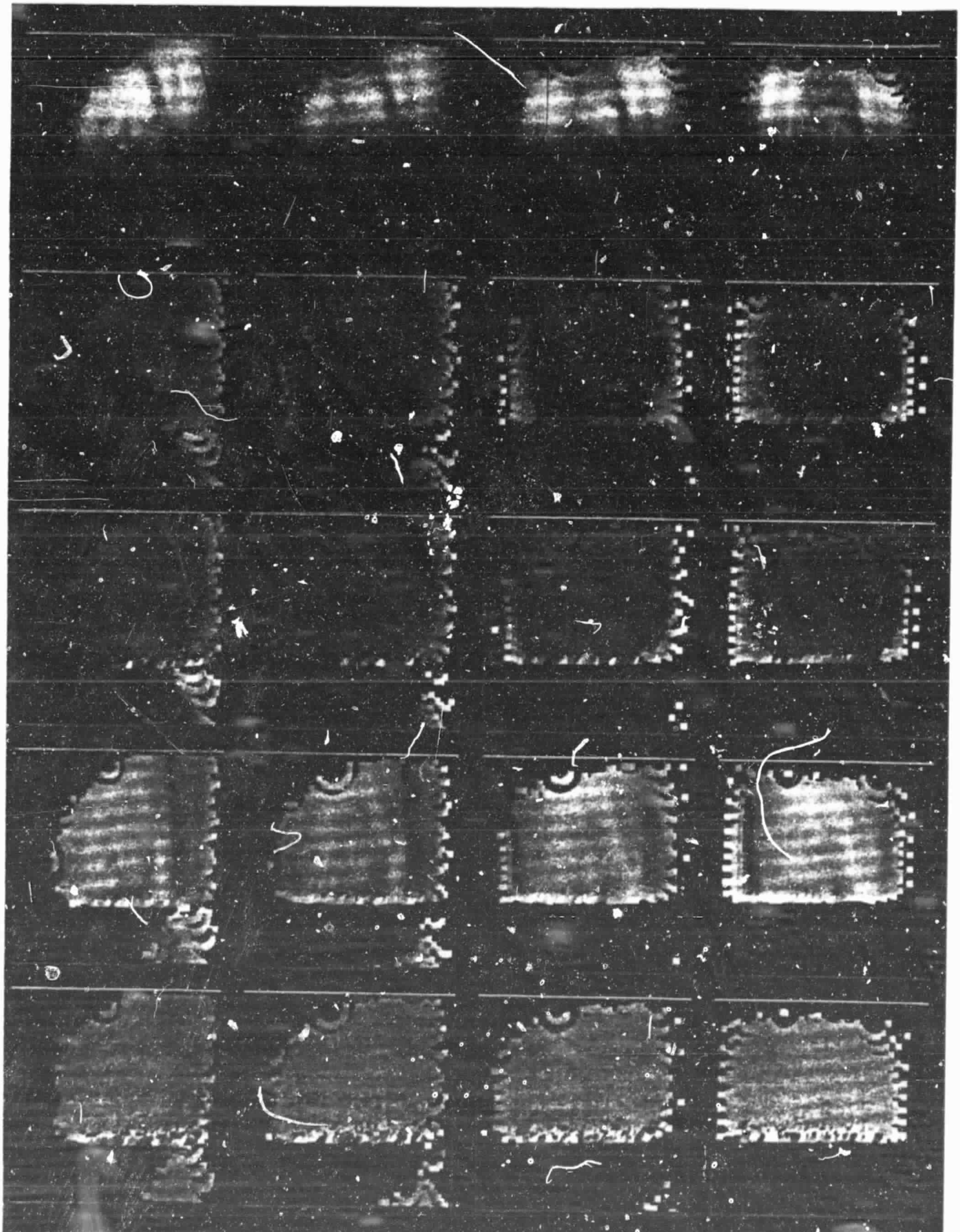

Figure 12d

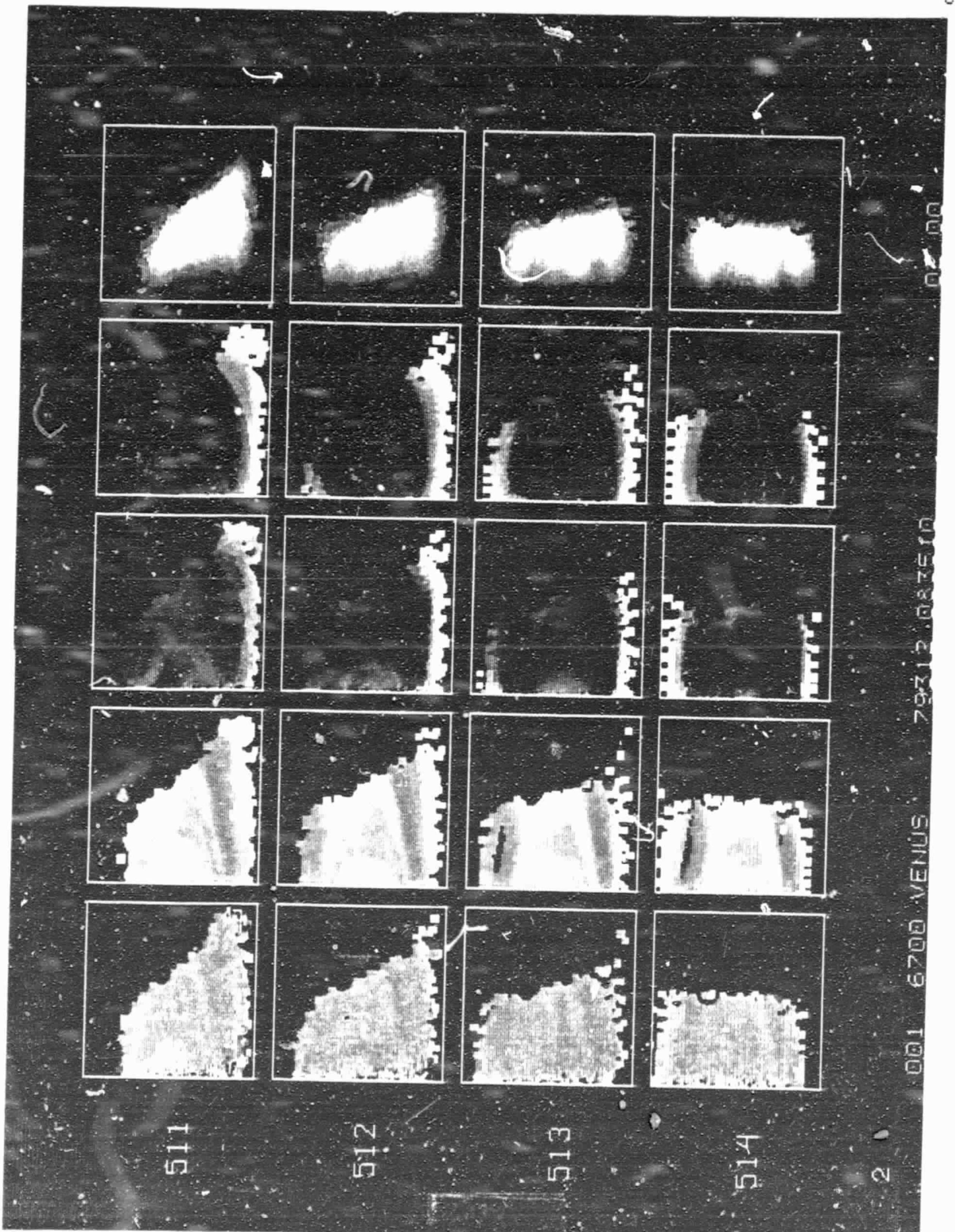

Figure 12e

ORIGINAL PAGE IS
OF POOR QUALITY

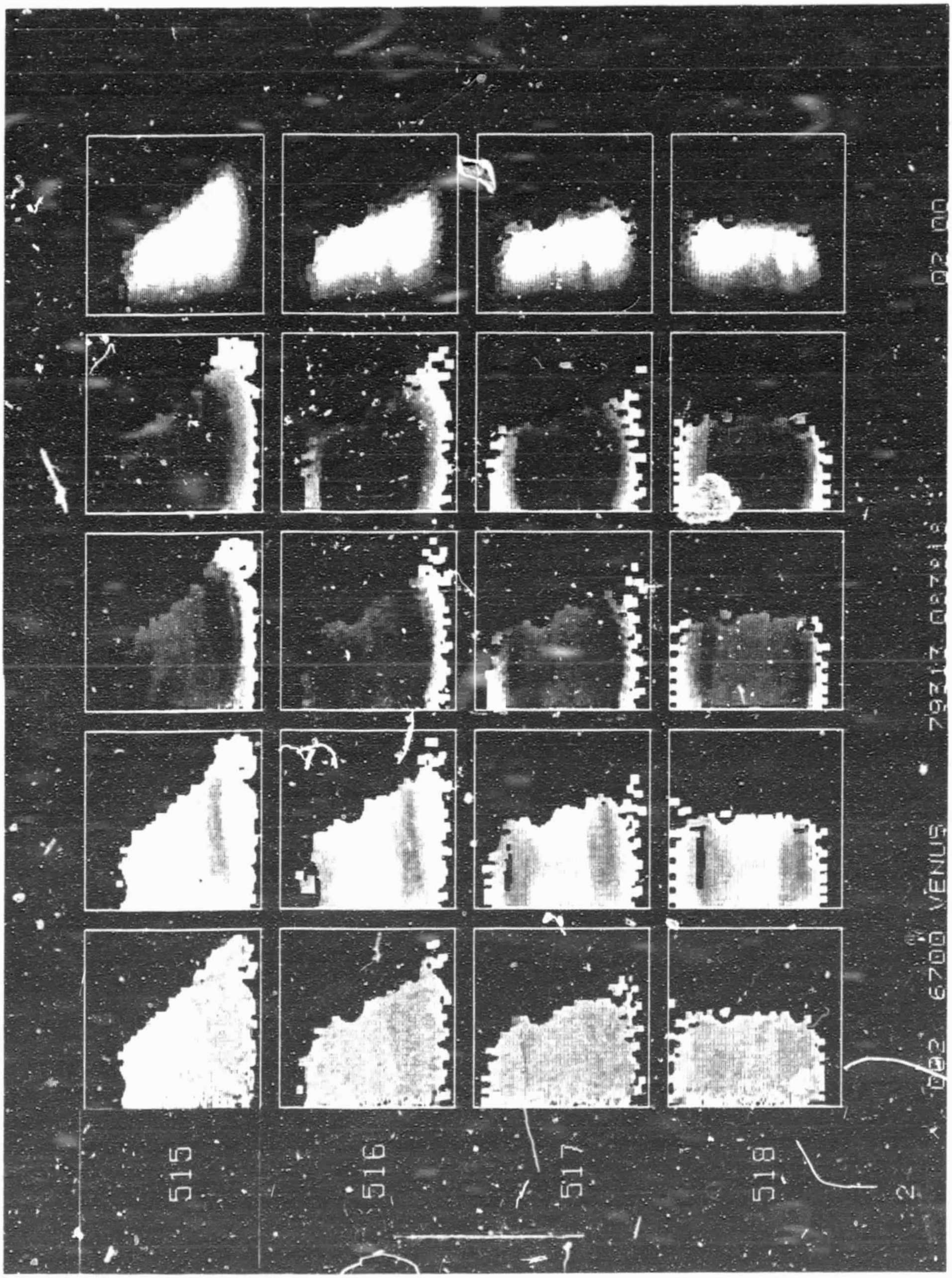

Figure 12f

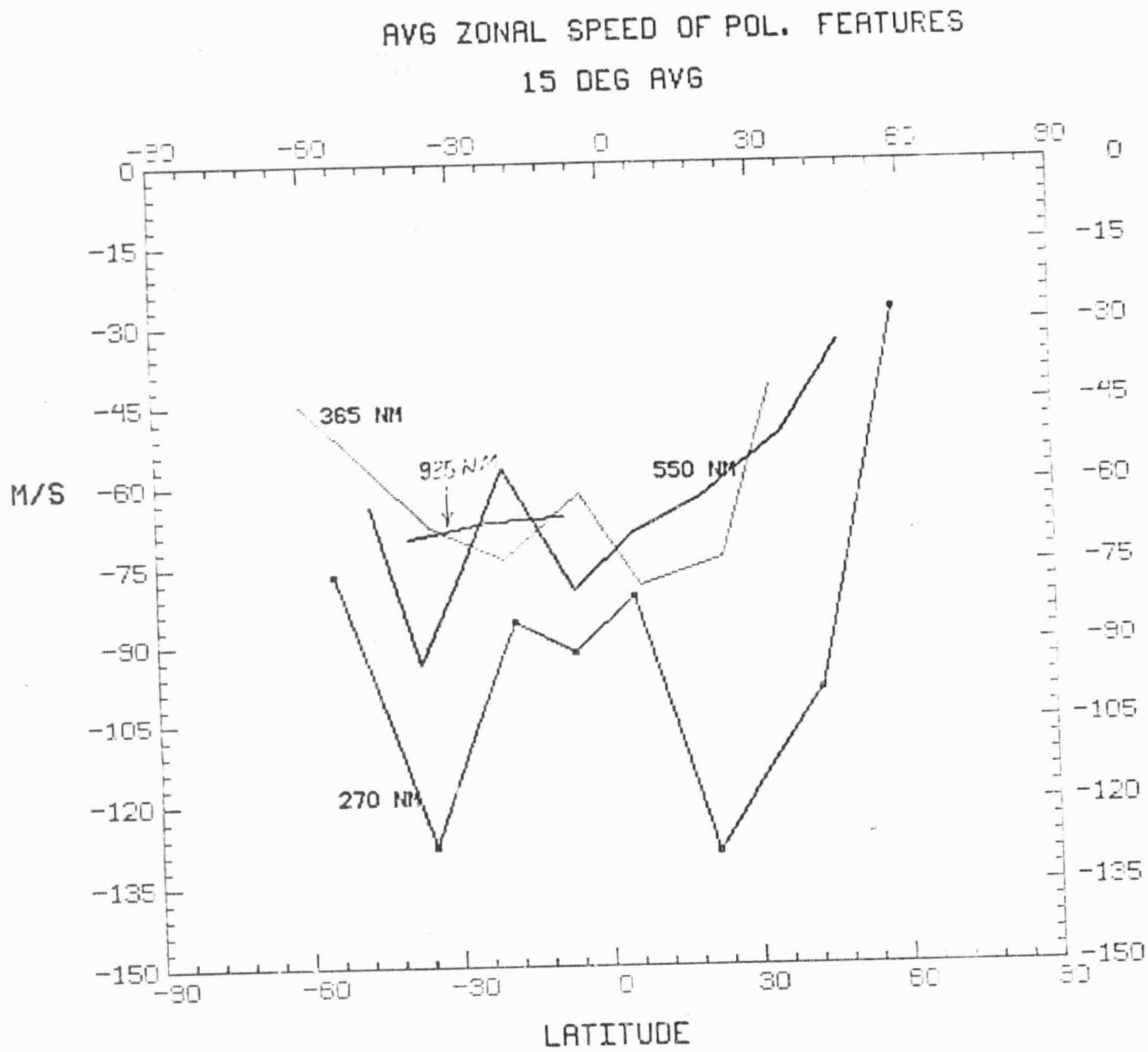
AVG ZONAL SPEED OF POL. FEATURES
15 DEG AVG
M/S
LATITUDE
365 NM
925 NM
550 NM
270 NM
-90 -60 -30 0 30 60 90
0 -15 -30 -45 -60 -75 -90 -105 -120 -135 -150

Figure 13